https://doi.org/10.5194/essd-2026-796
Preprint. Discussion started: 13 November 2026
© Author(s) 2026. CC BY 4.0 License.



Open Access Earth System Science Data Discussions

A database with refined plant functional type attribution at eddy covariance sites for enhanced land surface model simulations

Vincent Tartaglione[1,2,*], Fabienne Maignan[1,2], Vladislav Bastrikov[3], Philippe Peylin[1,2], Cédric Bacour[1,2]

[1]Laboratoire des Sciences du Climat et de l'Environnement (LSCE), CEA, CNRS, UVSQ, Université Paris-Saclay, Gif-sur-Yvette, France

[2]Institut Pierre-Simon Laplace (IPSL), Université de Versailles Saint-Quentin en Yvelines, Guyancourt, France

[3]Science Partners, 42 quai de Jemmapes, 75010 Paris, France

[*]*Correspondence to*: Vincent Tartaglione (vincent.tartaglione@protonmail.com)

Abstract. Measurements and estimates of carbon, water, and energy fluxes between the biosphere and the atmosphere, provided by eddy covariance (EC) techniques, are crucial to understand ecosystem functioning and for evaluating and improving land surface models (LSMs). Because most LSMs still rely on the vegetation description in the form of plant functional types (PFTs), accurate characterization of PFT fractions at EC sites

https://doi.org/10.5194/essd-2026-796
Preprint. Discussion started: 13 November 2026
© Author(s) 2026. CC BY 4.0 License.



is essential to reduce uncertainty in simulated fluxes, as well as in model parameters when EC data are used for calibration (data assimilation). However, the PFT information directly usable by LSMs is not provided by networks tower teams, leading to each LSM having its own methodology to prescribe PFTs.

This study presents a PFT attribution methodology and an associated database for 229 sites from the FLUXNET dataset and from regional networks, relying on the combination of multiple data sources, including literature review, information from network websites, satellite imagery, and a land cover map at 300 m. The resulting database of PFT fractions (based on 13 generic PFTs and 15 ORCHIDEE PFTs) across EC sites is associated with a confidence flag, based on the consistency between the various sources. Since *in situ* data do not always come with gap-filling information or can sometimes contain errors in the gap-filling process, we applied an automatic identification and removal of spurious data leading to a data coverage flag. Then, to assess the impact of this new PFT attribution on LSM simulations, we ran the ORCHIDEE LSM for simulating gross and net carbon fluxes, as well as energy fluxes. Those simulations led to the introduction of a model-data agreement flag (based on variability, correlation, and bias). The methodology, transposable to other LSMs with their own associated PFTs, provides a traceable framework for improving the PFT fractions attribution; the flags introduced aim at identifying the most relevant sites for validation and model calibration. The database is publicly available in CSV and XLSX format at https://doi.org/10.14768/6e99ff4b-3205-4038-8f9a-713e3e33753d (Tartaglione et al., 2026) and can be interactively explored at https://data.ipsl.fr/ecsitepftexplorer/.

https://doi.org/10.5194/essd-2026-796
Preprint. Discussion started: 13 November 2026
© Author(s) 2026. CC BY 4.0 License.



1 Introduction

Land Surface Models (LSMs) play a crucial role in our understanding of terrestrial-atmosphere interactions and are fundamental components of Earth System Models. These models use a functional representation of the vegetation through the concept of Plant Functional Types (PFTs), which group plant species with similar phenology, morphology and photosynthetic pathway, growing under similar climatic conditions (Prentice et al., 1992). The development of LSMs has largely been fueled by the parallel expansion of eddy-covariance sites (Williams et al., 2009; Pastorello et al., 2020), which provide *in situ* estimates of carbon, water, and energy fluxes between land ecosystems and the atmosphere. The quality and representativeness of these data, and the associated site characteristics, are therefore critical for evaluating fluxes simulated by LSMs. The assimilation of eddy-covariance fluxes has also been widely used for the calibration of LSM parameters (Kuppel et al., 2014; Raoult et al., 2016; Post et al., 2017; Abadie et al., 2023; Raoult et al., 2025). For these applications, a realistic estimate of the PFT fractions at each site is crucial to properly represent the contribution of the different PFTs to the observed fluxes. For data assimilation / parameter calibration, this is even more important to limit overfitting.

To prescribe PFT fractions for site level simulations, several sources of information can be used, but each comes with its own limitations. The main vegetation information provided by the different regional network websites such as ICOS (https://www.icos-cp.eu/, last access: 01 October 2026), AmeriFlux (https://ameriflux.lbl.gov/, last access: 01 October 2026), OzFlux (https://ozflux.org.au/, last access: 01 October 2026), AsiaFlux (https://asiaflux.nies.go.jp/, last access: 01 October 2026), etc., or the international FLUXNET network website (https://fluxnet.org/, last access: 01 October 2026), is an IGBP (International Geosphere-Biosphere Programme; Table S4) information most of the time, describing the dominant

https://doi.org/10.5194/essd-2026-796
Preprint. Discussion started: 13 November 2026
© Author(s) 2026. CC BY 4.0 License.



vegetation class, that is sometimes complemented by a description of the vegetation composition, species inventory or canopy structure. However, this information is not directly compatible with LSMs' needs, because it relies on a limited number of biome classes, which are often not directly mappable to models' PFTs. The process of mapping IGBP biome description into a limited set of PFT (typically of 10-15) remains a difficult task that relies on unformalised expert judgements and that is prone to specific and possibly biased choices, a caveat already identified in the community (e.g., (Marie et al., 2022; Wang et al., 2023)). *In situ* studies are sometimes using simplification by providing only the dominant PFT to represent the vegetation (e.g. (Stöckli et al., 2008; Peaucelle et al., 2019), possibly occulting vegetation heterogeneity.

For LSMS, an alternative approach is to rely on global land cover (LC) products, which are largely used for regional to global simulations, to derive PFT fractions based on cross-walking procedures that for instance map the 22 land cover classes of the United Nations Land Cover Classification System (UN-LCCS) (Di Gregorio and Jansen, 2001) into PFTs (Poulter et al., 2015; Harper et al., 2023a). Their spatial resolution is however not always compatible with site level scale and they may also fail to capture the true vegetation heterogeneity or correctly identify the dominant PFT of a given site.

These limitations are accentuated by the uncertainty of the actual footprint size and shape of eddy-covariance sites, which itself depends on atmospheric conditions as well as on the surrounding topography and vegetation of each site (Schmid, 2002; Kljun et al., 2015; Chu et al., 2021; Huang et al., 2022; Chu et al., 2026). The fractional cover of PFTs contributing to the measured fluxes then remains an important source of uncertainty that propagates to several key fluxes of carbon, water, and energy, simulated by LSMs (Hartley et al., 2017).

https://doi.org/10.5194/essd-2026-796
Preprint. Discussion started: 13 November 2026
© Author(s) 2026. CC BY 4.0 License.


Recently, Shi et al., (2025) released a dataset of site attributes (PFT fractions, soil texture, canopy height, LAI) for 90 EC sites, specifically for LSMs. Their study also shows that using refined PFT fractions instead of those derived from global land cover products has a significant impact on several simulated fluxes. This highlights the need for a consistent and reproducible approach for the attribution of PFT fractions at site level.

To address this need, we present a refined PFT fractions database for a large set of EC sites from major flux networks worldwide. Whereas Shi et al., (2025) addresses multiple attributes, we focus on the PFT attribution method, accounting for the vegetation heterogeneity and complementing the attribution with several flags. Our methodology derives site-specific PFT fractions by combining multiple information sources, including literature review, flux network metadata and high-resolution satellite imagery interpretation, within a transparent and traceable framework. The resulting database includes a "**confidence flag**" for each site, indicating the level of consistency found between the various sources.

This work was primarily motivated by the needs of the ORCHIDEE LSM community (Krinner et al., 2005), that uses *in situ* EC fluxes both for evaluation, and for data assimilation to calibrate key model parameters (Santaren et al., 2007; Bastrikov et al., 2018; MacBean et al., 2022; Bacour et al., 2023; Olivera-Guerra et al., 2025). However, the database provides PFT fraction expressed in terms of generic PFTs (a classification compatible with most LSMs following general principles based on life-forme, leaf-type and phenology, see §2.2.2). Each LSM can then further group some PFT (like shrub and tree), or split them according to specific climatic zone depending on their model specifications. In this regard we therefore also provide the fractions expressed in the 15 standard ORCHIDEE PFTs.

As part of the ORCHIDEE LSM calibration process, we regularly assimilate these *in situ* observations. However, the gap-filling information and quality control usually do not flag spurious data on the fluxes, which could

https://doi.org/10.5194/essd-2026-796
Preprint. Discussion started: 13 November 2026
© Author(s) 2026. CC BY 4.0 License.


lead to unrealistic data being assimilated. To address this issue, we developed an automatic procedure to detect spurious values and outliers and to quantify the completeness of measurements ("valid data"). This information is represented in the database by a "**data coverage flag**" indicating the proportion of valid measurements.

To assess the impact of the refined attribution of PFT fractions, we performed site-level simulations using the ORCHIDEE-v2 version (revision 4465) that was used for the CMIP (Coupled Model Intercomparison Project) Phase 6 climate simulations. These simulations allowed us to quantify model-data agreement for carbon and energy fluxes (variability, correlation, and bias), and we introduced a corresponding "**model-data agreement flag**".

This database (that comprise the 229 considered EC site list, along with their attributed PFT fractions) is publicly available at https://doi.org/10.14768/6e99ff4b-3205-4038-8f9a-713e3e33753d (Tartaglione et al., 2026). An associated website, available at https://data.ipsl.fr/ecsitepftexplorer/index.html (last access: 25 September 2026), also allows users to explore the EC sites with a datatable and a map, to visualize the time series of the flux data and the ORCHIDEE LSM simulations and to visualize satellite images of the surrounding area.

The paper is structured as follows. Section 2 describes the methodology for the PFT attribution, including the definition of the different PFT classes and EC sites considered, and the evaluation framework. The different data used for the attribution of the PFT fractions and for the evaluation are also described in this section. Section 3 details the results of the refined PFT fractions, showing the content of the resulting database and the impact of the refined PFT fractions on ORCHIDEE simulations. Section 4 describes the availability of the

https://doi.org/10.5194/essd-2026-796
Preprint. Discussion started: 13 November 2026
© Author(s) 2026. CC BY 4.0 License.


116 database, and presents the associated website developed to share this database. Section 5 of this study
117 discusses the pertinence and the limitations of the presented approach.

118 **2 Methodology**

119 **2.1 Eddy covariance sites**

120 The dataset includes 229 EC sites from the major networks ICOS (https://www.icos-cp.eu/, last access: 01
121 October 2026), NEON (https://www.neonscience.org/, last access: 01 October 2026), AmeriFlux
122 (https://ameriflux.lbl.gov/, last access: 01 October 2026), OzFlux (https://ozflux.org.au/, last access: 01
123 October 2026), and AsiaFlux (https://asiaflux.nies.go.jp/, last access: 01 October 2026). Most of them are
124 included in the global network FLUXNET, in the datasets of LaThuile (Baldocchi et al., 2001) and FLUXNET2015
125 (Pastorello et al., 2020). Others are from the ICOS WarmWinter2020 (Warm Winter 2020 Team, 2022) dataset.
126 This list of EC sites was initially made based on their relevance for the ORCHIDEE community. We excluded
127 the EC sites related to peatlands, wetlands, and crop rotation, as they cannot be accurately simulated with
128 ORCHIDEE-v2 that does not include these ecosystem specificities. We retained sites that have five
129 observations fluxes available: net ecosystem exchange (NEE), gross primary production (GPP), total
130 ecosystem respiration (TER), latent heat flux (LE) and sensible heat flux (H). Their spatial distribution is shown
131 in Fig. 1, with a majority of sites being in the Northern hemisphere and especially in Europe and North
132 America.

https://doi.org/10.5194/essd-2026-796
Preprint. Discussion started: 13 November 2026
© Author(s) 2026. CC BY 4.0 License.

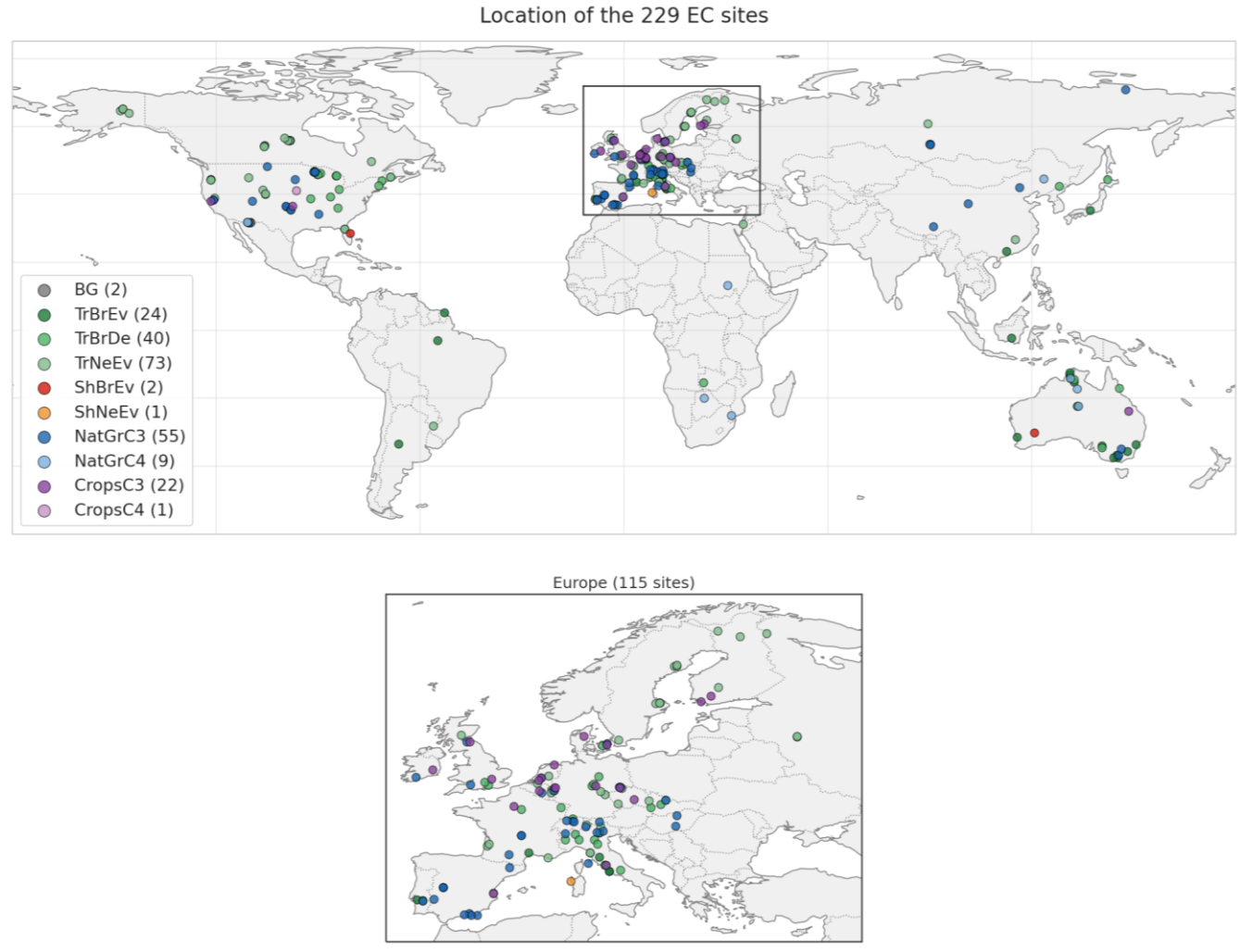


Figure 1: Location of the 229 EC sites, color-coded by dominant generic PFT. The inset shows Europe, where EC sites density is high.

2.2 PFTs classes

2.2.1 Generic PFTs

Generic PFTs refers to an LSM-independent vegetation classification derived from ESA CCI (Climate Change Initiative) LC classes (ESA, 2017), largely following the nomenclature by Poulter et al., (2015) and Harper et al., (2023a). Although initially developed for three LSMs, ORCHIDEE (Organising Carbon and Hydrology In

https://doi.org/10.5194/essd-2026-796
Preprint. Discussion started: 13 November 2026
© Author(s) 2026. CC BY 4.0 License.



Dynamic Ecosystems; (Krinner et al., 2005)), JULES (Joint UK Land Environment Simulator; (Best et al., 2011; Clark et al., 2011)) and JSBACH (Jena Scheme for Biosphere-Atmosphere Coupling in Hamburg; Reick et al., 2013), the resulting classification is relevant to many others LSMs. This classification groups vegetation by life form (tree/shrub/grass), leaf type (broadleaf/needleleaf), phenology (evergreen/deciduous) and management (natural/managed grasses), excluding attributes that require ancillary information such as climate or photosynthetic pathway.

In this study, we chose to add the C3/C4 photosynthesis mechanism partitioning for grasses and crops, since this distinction is used by many LSMs. The classification is described in Table 1.

Table 1: Generic PFTs and number of EC sites having the corresponding PFT as their main one (see §2.1).

Code	Description	Number of sites
BG	Bare Ground	2
TrBrEv	Broadleaf Evergreen Tree	24
TrBrDe	Broadleaf Deciduous Tree	40
TrNeEv	Needleleaf Evergreen Tree	73
TrNeDe	Needleleaf Deciduous Tree	0
ShBrEv	Broadleaf Evergreen Shrub	2
ShBrDe	Broadleaf Deciduous Shrub	0
ShNeEv	Needleleaf Evergreen Shrub	1
ShNeDe	Needleleaf Deciduous Shrub	0
NatGrC3	Natural Grassland (C3)	55
NatGrC4	Natural Grassland (C4)	9
CropsC3	Crops (C3)	22
CropsC4	Crops (C4)	1

https://doi.org/10.5194/essd-2026-796
Preprint. Discussion started: 13 November 2026
© Author(s) 2026. CC BY 4.0 License.



2.2.2 The ORCHIDEE model and its PFTs

ORCHIDEE is the land component of the IPSL (Institut Pierre Simon Laplace) Earth System Model (initially described in Krinner et al., (2005) with the version used in this study (ORCHIDEE-v2) and further described in Boucher et al., 2020), that computes the energy, carbon, and water exchanges between the land surface and the atmosphere. All components of the surface energy and water budgets, and photosynthesis, are calculated at a half-hourly time step; the carbon storage dynamics (including carbon allocation in plant reservoirs, soil carbon dynamics, and litter decomposition) are computed on a daily basis. All PFTs share the same equations but the parameters differ, except for the leaf phenology, which is based on various PFT dependent models (Botta et al., 2000).

While the generic PFTs group plants that have the same morphology and phenology, ORCHIDEE, as other LSMs, use a PFT classification that also accounts for climate. It uses Köppen-Geiger (KG) climate maps (Rubel et al., 2017) to introduce a distinction between tropical, temperate, and boreal climates, resulting in 14 vegetation PFTs plus one PFT for bare ground.

Table 2: ORCHIDEE PFTs and number of EC sites having the corresponding PFT as their main one (see §2.1).

Code	Description	Corresponding generic PFT	Number of sites
BG	Bare ground	BG	2
TroEBF	Tropical Evergreen Broadleaf Forest	TrBrEv, ShBrEv	9
TroDBF	Tropical Deciduous Broadleaf Forest	TrBrDe, ShBrDe	4
TemENF	Temperate Evergreen Needleleaf Forest	TrNeEv, ShNeEv	45
TemEBF	Temperate Evergreen Broadleaf Forest	TrBrEv, ShBrEv	17
TemDBF	Temperate Deciduous Broadleaf Forest	TrBrDe, ShBrDe	35

https://doi.org/10.5194/essd-2026-796
Preprint. Discussion started: 13 November 2026
© Author(s) 2026. CC BY 4.0 License.



BorENF	Boreal Evergreen Needleleaf Forest	TrNeEv, ShNeEv	31
BorDBF	Boreal Deciduous Broadleaf Forest	TrBrDe, ShBrDe	0
BorDNF	Boreal Deciduous Needleleaf Forest	TrNeDe, ShNeDe	0
TemC3GRA	Temperate natural C3 grassland	NatGrC3	39
C4GRA	Natural C4 grassland	NatGrC4	8
C3CRO	C3 cropland	CropsC3	22
C4CRO	C4 cropland	CropsC4	1
TroC3GRA	Tropical natural C3 grassland	NatGrC3	1
BorC3GRA	Boreal natural C3 grassland	NatGrC3	15

2.3 PFT fractions attribution steps

The information about the vegetation cover of the EC site is documented heterogeneously across sites and networks. To attribute consistent PFTs, we thus combined information about the vegetation from multiple sources, including network websites, PI reports, literature, and imagery. We tried as much as possible to be systematic, and avoid unsupported attributions, and to rely on our expert judgement only when sources were too inconsistent. We first mapped the text information to generic and ORCHIDEE-specific PFTs. Then, the resulting PFTs fractions were refined using satellite and ground-level imagery. We then used reference products to evaluate and potentially correct the obtained fractions. The PFT fractions attributed to the EC sites have been shared with each PI and have been corrected when needed. This procedure is summarized in Fig. 2 and detailed in the following sub-sections.

https://doi.org/10.5194/essd-2026-796
Preprint. Discussion started: 13 November 2026
© Author(s) 2026. CC BY 4.0 License.

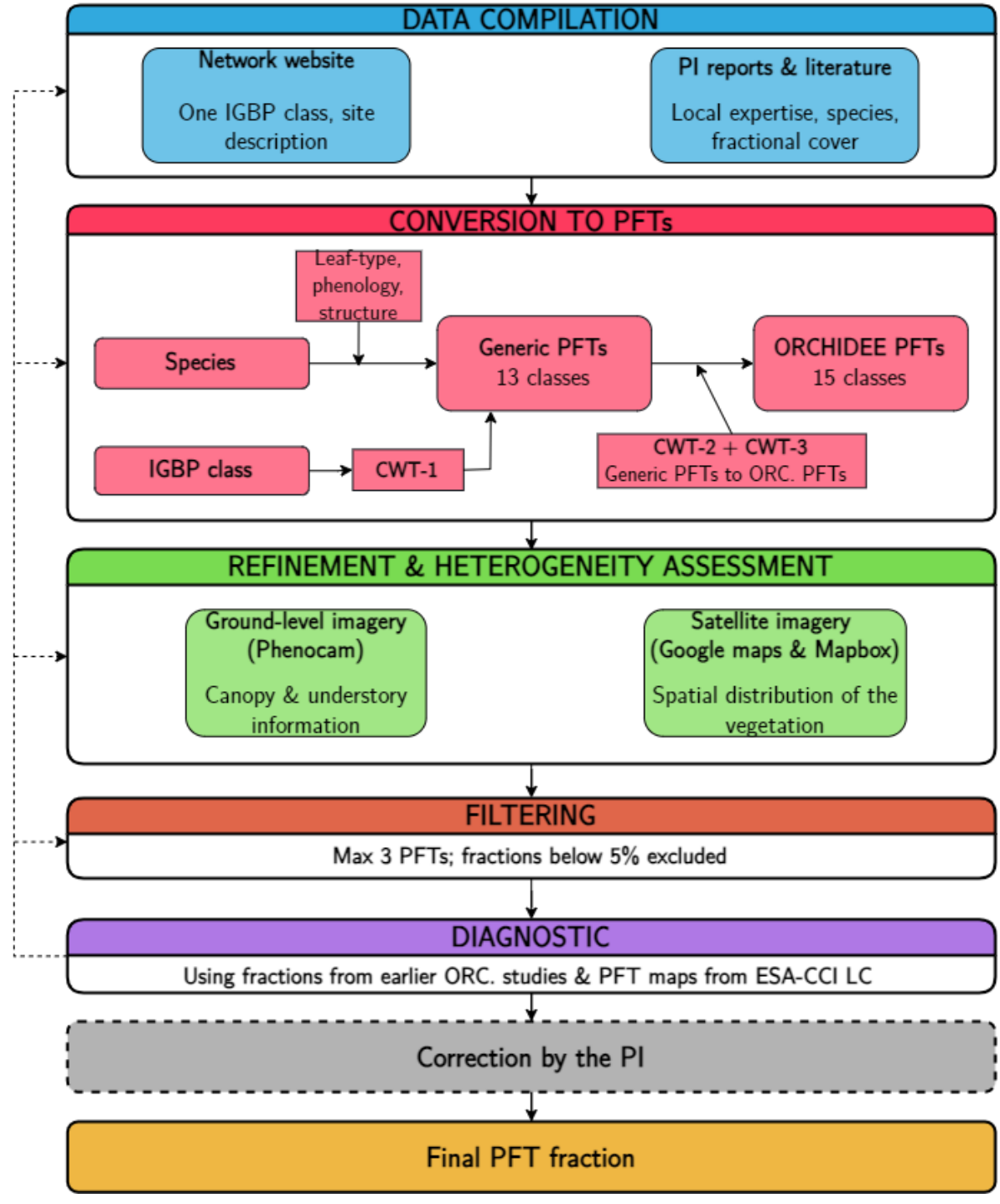


Figure 2: Overview of the PFT attribution steps.

https://doi.org/10.5194/essd-2026-796
Preprint. Discussion started: 13 November 2026
© Author(s) 2026. CC BY 4.0 License.


2.3.1 Network information sources

Most of the EC sites are provided, on their associated network website, with the main vegetation type, often in terms of one IGBP class. A site description can also give more detailed information concerning the vegetation species present in the surrounding area, and sometimes with the approximate proportion of the site covered by the main vegetation species. Further detail can come from PI reports (often referenced in the EC site's webpage), and from literature, with local expertise.

2.3.2 Cross-walking tables

The conversion between land cover and PFT classifications relies on CWTs, which establish a correspondence between the classes from a source classification and those of a target classification, sometimes conditioned to ancillary information such as the climate zone (cross-walking tables and mapping algorithms documented at https://orchidas.lsce.ipsl.fr/dev/lccci/tools.php, last access: 9 June 2026).

We used three CWTs in this study: CWT-1 to map IGBP classes to generic PFTs (see **§2.3.3**), CWT-2 accounting for climate zones to convert generic PFTs to ORCHIDEE PFTs (see **§2.3.3**), and CWT-3 to aggregate 31 Köppen-Geiger climate classes (KG31) into 7 ORCHIDEE climate classes (KG7) (see §**2.3.5**).

2.3.3 Conversion to generic and ORCHIDEE PFTs

The species list, when available, was assigned to generic PFTs, depending on the leaf-type (broadleaf/needleleaf), phenology (evergreen/deciduous), structure (tree/shrub/grass) and C3/C4 partitioning. The information of their proportion, when provided, was used for defining the generic PFTs fractions. Otherwise, when only the IGBP class of the main vegetation was provided, it was mapped to generic PFTs using CWT-1 (Table S1). For some classes this mapping is direct (for example, 'ENF' or 'DBF' maps

https://doi.org/10.5194/essd-2026-796
Preprint. Discussion started: 13 November 2026
© Author(s) 2026. CC BY 4.0 License.


199 respectively to at least 60% of TrNeEv and 60% of TrBrDe), and imagery (see §**2.3.4**) was used to determine
200 the remaining PFT fractions. For other classes such as 'SAV', 'CVM' or 'CSH', several generic PFTs can be
201 compatible, and further information is needed to determine the PFTs: leaf-type (that can partly be
202 determined using imagery) and C3/C4 partitioning (inferred from ancillary products, see §**2.3.5**).
203 The generic PFTs were then mapped onto ORCHIDEE PFTs using CWT-2 (Table S2). As the ORCHIDEE PFTs
204 depend on the ORCHIDEE climate classes, the Köppen-Geiger class was first converted from KG31 to KG7
205 using CWT-3.
206 The result of this step gives the main generic/ORCHIDEE PFT(s), it can be a single PFT or PFT fractions. This
207 attribution is then refined and the heterogeneity assessed with visual information of the sites using ground-
208 level and satellite imagery.

209 **2.3.4 Local heterogeneity assessment**

210 The PFTs resulting from the previous step do not always represent the actual heterogeneity, in terms of PFT
211 fractions, in the fluxtower surrounding area, especially for EC sites with sparse information (e.g. only the IGBP
212 class). This heterogeneity was therefore assessed using ground level images on canopy and understory from
213 phenocam photographs (https://phenocam.nau.edu/webcam/, last access: 9 June 2026), combined with
214 satellite images for all sites. Furthermore, when information on vegetation was limited, these images helped
215 determine a generic PFT class, based on the visibility of the leaf-type and structure of the vegetation (mainly
216 broadleaf or needleleaf, herbaceous or tree). The flux footprint, which is the source area that contributes to
217 the flux measurements, typically extends hundreds of meters to a kilometer around the tower depending on
218 measurement height, wind conditions, vegetation cover, atmospheric stability (Kljun et al. 2015; Huang et al.,
219 2022; Chu et al., 2021; Chu et al., 2026) and the contribution of the vegetation to measured flux decrease with

https://doi.org/10.5194/essd-2026-796
Preprint. Discussion started: 13 November 2026
© Author(s) 2026. CC BY 4.0 License.


distance. Because deriving the footprint of each EC site was beyond the scope of this study, we adopted an identical fixed extent approach for all the considered EC sites in order to assess the heterogeneity within the surrounding area of each flux tower. We developed a Python script that retrieves two satellite images from Google maps (https://www.google.fr/maps/, last access: 23 June 2026) and from Mapbox (https://www.mapbox.com/imagery, last access: 23 June 2026) for each site because for some sites, the image from one provider was either unavailable or of bad quality. The two satellite images were centered on the EC site coordinates, at two spatial extents: a close view targeting a width of ~350 m for the main contributing vegetation and a wider view targeting a width of ~1500 m for the landscape information and distant vegetation. Because Google maps and Mapbox only accept integer zoom levels (parameter that sets the spatial scale of the retrieved images), the actual ground extent varied across sites, from ~250 to ~500 m (~0.3 to 0.6 m/pixel for a 800x800 image) for the close view and from ~1000 to ~2000 m (~1.3 to 2.5 m/pixel for a 800x800 image) for the wider view. The zoom level was computed from the site's latitude to compensate for the distortion of the projection. The resulting extent was then overlaid on each image together with the site name and coordinates (Fig. 3).

We limited the final PFT fractions to a maximum of three PFTs and fractions below 5% were removed, the remaining fractions normalised.

https://doi.org/10.5194/essd-2026-796
Preprint. Discussion started: 13 November 2026
© Author(s) 2026. CC BY 4.0 License.



Figure 3: Close extent (261 m) (left) and wide extent (1045 m) (right) images of the site BE-Bra: Brasschaat (51.3076°N, 4.5198°E). The EC site provider indicates that "the study site consists of a 2 ha, even-aged Scots pine stand (Pinus sylvestris L.) situated within a 150 ha mixed coniferous/deciduous forest dominated by Scots pine". The close view shows the predominant presence of TrNeEv as the main contributing vegetation, with patches of TrBrDe. The wide view shows the presence of grasslands a few hundred meters from the flux tower and other trees stand, likely within the footprint given the 40 m tall tower. We classified this site as TrNeEv (0.80), TrBrDe (0.10), NatGrC3 (0.10). Imagery from Google and data providers as indicated on the image.

2.3.5 Refinement against reference PFT products

We compared the ORCHIDEE PFT fractions to those considered in previous ORCHIDEE studies: those defined for the PLUMBER2 project (Abramowitz et al., 2024) and those defined for ORCHIDEE-CCDAS (Peylin et al., 2016; Bacour et al., 2023), for a subset of 142 common sites, and to those inferred from a global reference PFT map at 300 m, to diagnose potential issues in the attribution process.

Regarding the reference map, we used the 300 m annual PFT maps from Harper et al. (2023a), which is derived from the ESA CCI medium-resolution land cover (MRLC) dataset and is available at

https://doi.org/10.5194/essd-2026-796
Preprint. Discussion started: 13 November 2026
© Author(s) 2026. CC BY 4.0 License.


https://doi.org/10.5285/26a0f46c95ee4c29b5c650b129aab788 (Harper et al., 2023b). This product provides global fractional covers in terms of 14 generic PFTs for the years 1992-2020. We used the middle year of the measurement period of each EC site.

We derived ORCHIDEE PFTs fractions at each of the EC sites from this product in combination with three ancillary datasets:

1) a C3/C4-partitioning map at 1/6° resolution (Still et al., 2009) to separate fractions of natural herbaceous by photosynthetic pathway, resampled at 0.0125° resolution;
2) the LUH2 (Land Use Harmonization) dataset at 0.25° of resolution (Chini et al., 2021; Hurtt et al., 2020) to distinguish crop types, resampled at 0.0125° resolution;
3) the Köppen-Geiger (KG) climate map at 5 arc minutes (~0.0833°) of resolution (Rubel et al., 2017) that assigns the climate zone based on temperature and precipitation, resampled to 0.0125° resolution for 7 classes.

These four datasets were merged at each EC site coordinates using CWT-2 to derive the ORCHIDEE PFT fractions at the EC sites coordinates nearest grid cell.

These two references were used to identify possible misattributions, allowing us to re-examine our attribution process, not as validation. Note that the ORCHIDEE PFTs derived from the global CCI product are not always representative at the site-scale: for example, the site US-Ha1 (Harvard Forest EMS Tower) is classified as a temperate evergreen needleleaf forest (TemENF) while being a temperate deciduous broadleaf forest (TemDBF). The PFTs used in previous ORCHIDEE studies are a more reliable reference, but the attribution is not documented. When a substantial disagreement was found (e.g. a different dominant PFT), we reviewed our attribution and revised it if we identified an error on our side. In case of any revision

https://doi.org/10.5194/essd-2026-796
Preprint. Discussion started: 13 November 2026
© Author(s) 2026. CC BY 4.0 License.


identified on the ORCHIDEE PFT fractions, we propagated the revision to the corresponding generic PFT (see Table 2), by splitting Tree/Shrub using the network's information if available or the imagery (§**2.3.4**)

2.3.6 Confidence flag definition

For each site we assigned a confidence flag (A → C) to summarise the reliability of the attributed PFT fraction. This flag reflects the number of available information (network metadata, PI reports, literature, imagery), the level of agreement across sources and the degree to which the attributed PFTs relied on expert judgment.

A (high confidence): Multiple sources agree on the main corresponding generic PFT and fractions, the imagery is consistent with the metadata and the attribution required little expert judgment.

B (medium confidence): Sources show minor discrepancies, or one important source is missing but the other sources are consistent.

C (low confidence): Sources show major discrepancies (e.g. different main corresponding generic PFT) or the attribution rests on limited information (e.g. only IGBP class).

2.4 Evaluation

2.4.1 Data cleaning and quality assessment

The standard approach to gap-fill data for EC data uses the marginal distribution sampling (MDS) (Reichstein et al., 2005) and neural networks (Moffat et al., 2007), as implemented in the ONEFlux processing pipeline (Pastorello et al., 2020). For meteorological fields, this gap-filling also uses the MDS method, with downscaled meteorological reanalysis products (ERA-Interim, Dee et al, 2011; ERA5, Hersbach et al. 2023 for recent releases of FLUXNET data), as an alternative to low quality gap-filling. Data providers give the gap-filling information for meteorological fields using an integer (0 - 2) indicating "measured", "high quality with MDS",

https://doi.org/10.5194/essd-2026-796
Preprint. Discussion started: 13 November 2026
© Author(s) 2026. CC BY 4.0 License.


293 "ERA downscaled" and for carbon, energy and water measured fluxes using an integer (0 - 3) indicating
294 "measured", "good confidence", "medium confidence" or "low confidence", based on the availability of the
295 drivers used in the MDS method.
296 However, the latest versioned ORCHIDEE formatting script retained only a flag for gap-filled meteorological
297 fields, encoded as a binary value (gap-filled / measured). Gap-filling can produce realistic values.
298 Nevertheless, errors in the processing steps can introduce spurious values, in the form, for example, of
299 constant or flat patterns over several time steps (days), as shown in Fig. 4. We therefore developed an
300 automatic filtering process to detect and remove these spurious data directly from the flux time series. The
301 analysis was performed on daily aggregated fluxes of net ecosystem exchange (NEE), gross primary
302 production (GPP), total ecosystem respiration (TER), latent heat flux (LE) and sensible heat flux (H).
303 The filtering followed these successive steps:
304 • It first removed unrealistic values. To do so, we applied specific bounds to each variable. For carbon
305 fluxes (NEE, GPP and TER), values outside the range -100 to 100 $gC.m^{-2}.d^{-1}$ and for energy fluxes (LE
306 and H), values outside - 500 to 500 $W.m^{-2}$, were considered non-physical and were removed.
307 • Then, the algorithm detected repeating patterns or constant values, at a daily resolution. It compared
308 adjacent subsets of the time series of fixed length of 12 days (short patterns) and 21 days (long
309 patterns). For each consecutive subsets, the data were detrended and the resulting sequences were
310 compared element-wise. Two subsets were considered highly similar if the absolute difference
311 between the corresponding values was smaller than a threshold dependent on the data range after
312 the removal of the non-physical values (0.1% for the short patterns and 1% for the long patterns).
313 Periods that exhibited highly similar patterns were flagged. In addition, the algorithm flagged periods

https://doi.org/10.5194/essd-2026-796
Preprint. Discussion started: 13 November 2026
© Author(s) 2026. CC BY 4.0 License.



with very low variability using a rolling standard deviation over a period of six days. Values were flagged as constant when this standard deviation was below one ten-thousandth of the data range. For carbon fluxes, this constant-pattern mask was derived from NEE and applied jointly to NEE, GPP and TER. For energy fluxes, it was derived from H and applied to H and LE. The flagged segments were then treated as missing data.

- Finally, a specific processing was applied for winter peaks (winter is defined based on latitude and day of year) for GPP and TER, since these fluxes may be subject to unphysical high values during this season that are not caught during the first step as their amplitude may still be lower than typical summer values. Within these periods, flux values were compared to the median winter value using a modified Z-score (Iglewicz and Hoaglin, 1993), defined as $Z_i = \frac{0.6745(x_i - \hat{x})}{MAD}$, where $\hat{x} = median(x)$ and $MAD = median(|x_i - \hat{x}|)$ is the median absolute deviation. Observations with $Z > 10$ (corresponding to ~15 times the median absolute deviation) were flagged. A complementary approach was also applied using a rolling median and a rolling MAD over a shorter 15-day window, with a Z-score threshold of 5 for GPP and 4 for TER, corresponding respectively to 7.5 and 6 MAD.

The different parameters such as window lengths and detection thresholds are the same for all the sites and were fixed empirically by an iterative approach ensuring the removal of a maximum of unphysical values while preserving the variability of the measures.

https://doi.org/10.5194/essd-2026-796
Preprint. Discussion started: 13 November 2026
© Author(s) 2026. CC BY 4.0 License.

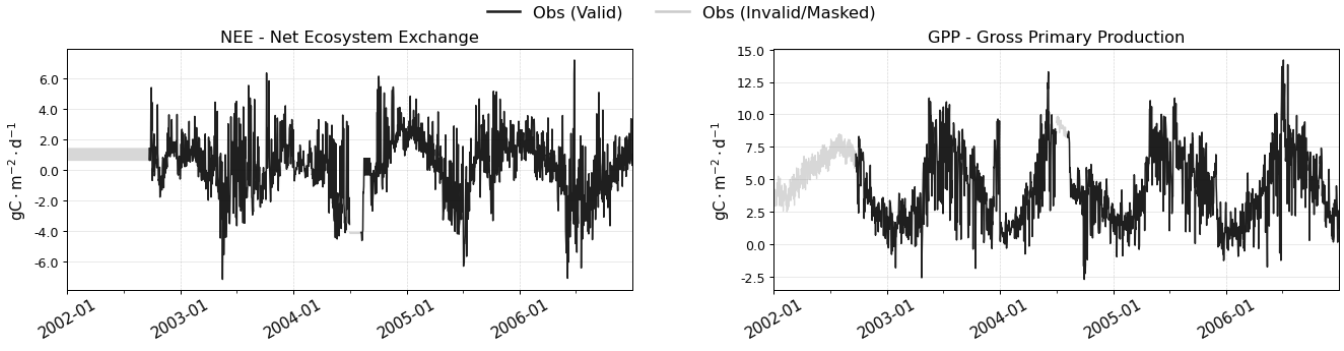


Figure 4: Example of filtered EC data (in grey) on the site JP-SMF for the variables NEE and GPP.

2.4.2 Assessment of the model-data agreement with ORCHIDEE simulations

By comparing the simulations of NEE, GPP, TER, LE, and H fluxes at the 229 sites performed with ORCHIDEE, considering either the newly defined PFT fractions or only the dominant PFT, we were able to assess the impact of the PFT refinement. We used ORCHIDEE in offline mode, in which atmospheric conditions were given by the local meteorological forcing files. The simulations were performed at a half-hourly time step, and fluxes analyzed at a daily-mean resolution. The soil texture was derived from the FAO-USDA (Food and Agriculture Organization of the United Nations–United States Department of Agriculture) map representing twelve classes (Reynolds et al., 2000). The model spinup was performed by cycling the forcing with the CO_2 level of the year 1860 followed by a transient simulation using the CO_2 from the year 1861 to the first year of the forcing file, using the built-in analytical spinup based on Lardy et al. (2011).

2.4.3 Data quality flags

We provide two additional flags to assess the confidence in the data at each site qualitatively, and relative to the ORCHIDEE model: a “data coverage flag” and a “model-data agreement” flag. These flags are based on the five fluxes considered in this study (NEE, GPP, TER, LE and H).

https://doi.org/10.5194/essd-2026-796
Preprint. Discussion started: 13 November 2026
© Author(s) 2026. CC BY 4.0 License.



Data coverage flag (a → d): For each variable, we computed the proportion of data which was flagged as invalid over the available time series, leading to a data coverage flag per variable according to the thresholds of Table 3. A global coverage flag is derived from the average proportion across the five variables and following the same thresholds.

Table 3: Data coverage flag thresholds.

Flag	Data coverage
a	90-100%
b	70-90%
c	50-70%
d	<50%

Model-data agreement flag (1 → 4): For each variable, we normalized simulated and observed fluxes time series using the 5th-95th percentile range of the observations. Using three metrics following the decomposition used in Taylor diagrams (Taylor, 2001): correlation (R), variability ratio ($\sigma_{model}/\sigma_{obs}$, σ denoting the standard deviation) and absolute bias, we computed a model-data agreement flag, according to the thresholds of Table 4, where a given flag was attributed only if all three metrics simultaneously satisfied the threshold. For a given site, the overall model-data agreement flag was computed as the mean of the individual flags across the five fluxes, rounded to the nearest integer, with half values rounded to the better (lower) flag.

Table 4: Model-data agreement flag thresholds.

Flag	Correlation	Variability ratio	Abs. bias
1	≥ 0.8	0.8 - 1.2	≤ 0.1
2	≥ 0.6	0.6 - 1.4	≤ 0.2
3	≥ 0.4	0.4 - 1.6	≤ 0.3
4	< 0.4	< 0.4 or > 1.6	> 0.3

https://doi.org/10.5194/essd-2026-796
Preprint. Discussion started: 13 November 2026
© Author(s) 2026. CC BY 4.0 License.



3 Results

3.1 Database format and content

The resulting database is a table in CSV/XLSX format, available at https://doi.org/10.14768/6e99ff4b-3205-4038-8f9a-713e3e33753d (Tartaglione et al., 2026). The fields and field descriptions are detailed in Table 5. This table contains standard site metadata (identifier, name, coordinates, and network), vegetation expressed as generic PFTs and ORCHIDEE PFTs (dominant and fractions), as well as additional fields with the three flags, the list of the sources of information considered for the definition of the PFT fractions, and the climate zone. For each site, we compiled references to site descriptions, PI reports, and related publications, which provide the most reliable information concerning species composition, management, disturbance history, and footprint context. In addition to the vegetation fractions and flags, optional notes can be provided that synthesize information from these sources about the main vegetation species, management conditions, particular events, or any other relevant information constraining the PFT attribution.

Table 5: Database field description.

Field	Description
site_id	Site identifier - COUNTRY-Site code (e.g. FR-Fon).
name	Site name (e.g. Fontainebleau-Barbeau).
lat	Latitude, decimal degrees, WGS84
lon	Longitude, decimal degrees, WGS84
dominant_orchidee_pft	Dominant ORCHIDEE PFT code, e.g. “PFT06” (TemDBF).

https://doi.org/10.5194/essd-2026-796
Preprint. Discussion started: 13 November 2026
© Author(s) 2026. CC BY 4.0 License.



orchidee_pft_fraction	ORCHIDEE PFT fractions; fractions sum to 1, e.g. "PFT06(0.90), PFT10(0.10)" (TemDBF(0.90), C3GRA(0.10)).
dominant_generic_pft	Dominant generic PFT code, e.g. "TrBrDe" (Broadleaf Deciduous Tree).
generic_pft_fraction	Generic PFT fractions; fractions sum to 1, e.g. "TrBrDe(0.90), NatGrC3(0.10)".
igbp	IGBP land cover class
koppen_geiger	Köppen-Geiger climate class (KG7)
confidence_flag	PFT attribution confidence: A - C.
data_coverage_flag	Flux data coverage flag: a - d.
model_data_agreement_flag	ORCHIDEE model-data agreement flag: 1 - 4.
sources	Reference URLs & references used for the attribution.
dataset	Source flux dataset(s), e.g. FLUXNET2015, FLUXNET2007.
network/hub	Source network, e.g. AmeriFlux, ICOS.
citation	Short form of the reference e.g. "Author et al., year"
reference	Full citation of the flux data used with DOI
remarks	Free-text notes (species, management history, etc.).
year_fluxnet2007	Years of data availability in FLUXNET2007 (LaThuile). Empty: not in that dataset.
year_fluxnet2015	Years of data availability in FLUXNET2015. Empty: not in that dataset.

https://doi.org/10.5194/essd-2026-796
Preprint. Discussion started: 13 November 2026
© Author(s) 2026. CC BY 4.0 License.



year_warmwinter2020	Years of data availability in Warm Winter 2020. Empty: not in that dataset.

3.2 Flags distribution across the database

Most sites exhibit at least high confidence (>= B) in their attribution of PFT fractions. Figure 5 shows the distribution of the different flags across all 229 sites:

- 58.5% of the sites (134) are classified with the best confidence « High », indicating strong consistency between the different sources of information (network metadata, literature, and satellite imagery, PI review).
- 34.9% of the sites (8) fall under the second confidence flag « Medium », corresponding to minor discrepancies among sources.
- 6.6% (15) are assigned flag “C”, which reflects larger uncertainties or limited information availability.

The data coverage flag shows that 85.2% of sites have a high proportion of valid data (flags a or b). The model-data agreement flag with the refined PFT fractions, based on correlation, variability ratio, and bias, shows that 38% of sites achieve excellent or good agreement (flags 1 or 2) between observed fluxes and those

https://doi.org/10.5194/essd-2026-796
Preprint. Discussion started: 13 November 2026
© Author(s) 2026. CC BY 4.0 License.

simulated with ORCHIDEE. The detailed results are summarized in the bar plots of Fig. 5.

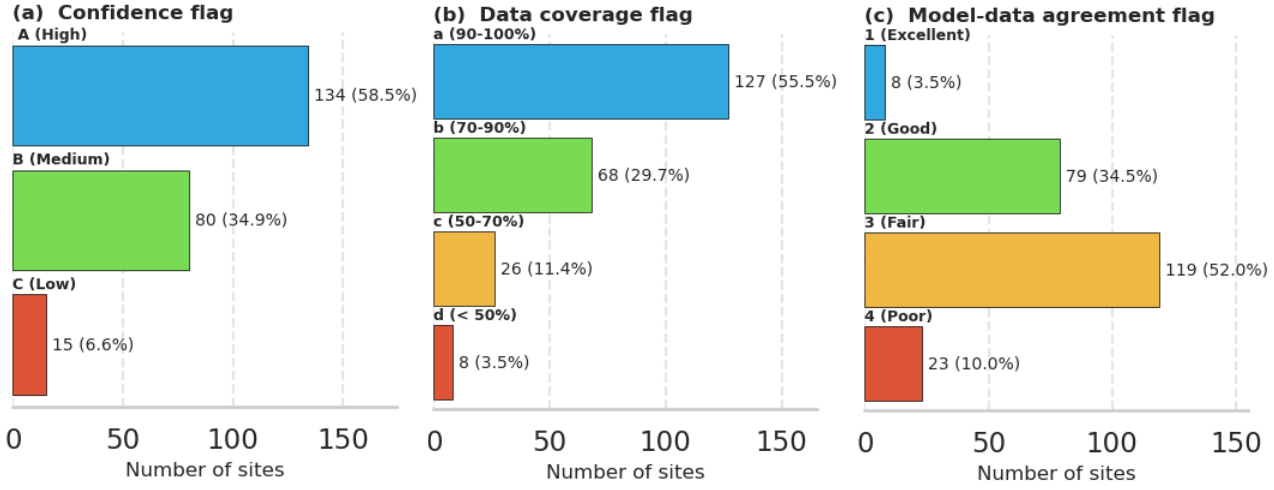


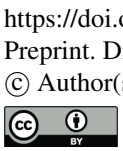
Figure 5: Distribution of (a) the confidence flag; (b) the data coverage flag; (c) the model-data agreement flag, for their different flags. For each flag are provided the number of sites and the percentage (across 229 sites).

3.3 Impact on ORCHIDEE simulations

We compared the simulated fluxes between two experiments: one in which the refined PFT fractions was used and one considering only the dominant PFT (referred to as “pure” PFT later on). Since the two experiments were identical for sites whose dominant PFT fraction approaches 1, we restricted the comparison to sites whose dominant PFT fraction is lower than 0.95 and we excluded the site with bare ground (BG) as dominant PFT (187 sites out of 229).

Figure 6 compares the model-data agreement flags for each of the five fluxes, obtained in each experiment. It quantifies how many sites have a different agreement flag between both experiments. Except for the sensible heat flux *H*, accounting for vegetation heterogeneity (i.e. using the refined PFT fractions) improves the model-data agreement overall (more sites in the “improve” region on the matrix, below the diagonal).

https://doi.org/10.5194/essd-2026-796
Preprint. Discussion started: 13 November 2026
© Author(s) 2026. CC BY 4.0 License.



Open Access Earth System Science Data Discussions

Most of the sites however have the same flag because the differences between the two experiments are smaller than the width of the flag thresholds, as detailed in Table 6.

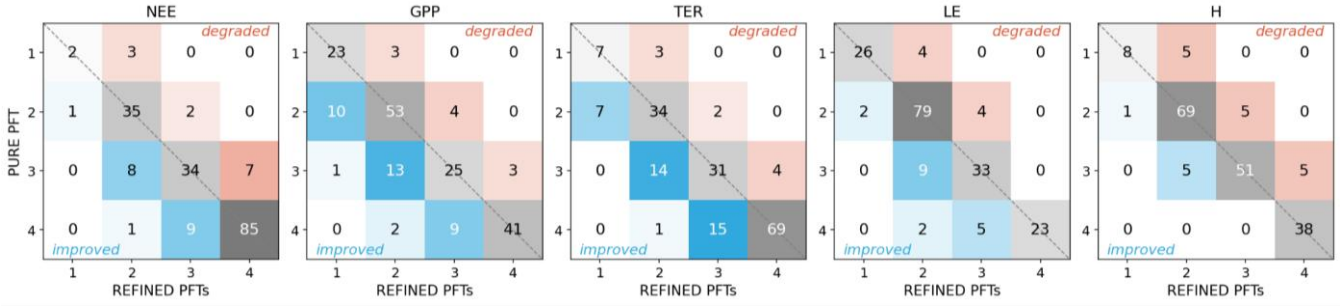


Figure 6: Comparison of the model-data agreement flags for NEE, GPP, TER, LE and H, obtained with the two experiments (refined PFTs vs pure PFT). Each flag cell indicates the number of sites. Blue scale indicates a better agreement flag with the refined PFTs. Red scale indicates a better agreement with the pure PFT. Grey scale indicates an identical agreement flag between both approaches.

Table 6: Comparison of the total number of sites with a better agreement flag between the two experiments for each variable.

	NEE	GPP	TER	LE	H
Same flag	156	142	141	161	166
Better agreement with refined PFTs	**19**	**35**	**37**	**18**	6
Better agreement with pure PFT	12	10	9	8	**15**

We then compared the three metrics considered for the definition of the model-data agreement flag (the correlation, variability ratio and absolute normalized bias differences (Refined - Pure)) in Fig. 7 for each PFT and flux. Since the variability ratio is better when it is closer to 1, we compute the absolute differences of the deviation from 1. For the bias, absolute values are considered. For each metric, each cell of the diagram shows

https://doi.org/10.5194/essd-2026-796
Preprint. Discussion started: 13 November 2026
© Author(s) 2026. CC BY 4.0 License.



the mean across all sites for a given ORCHIDEE PFT and flux variable. While the refined PFTs improve the correlation and the variability ratio for almost all PFTs and fluxes, the impact on the bias is more balanced, with improvements (absolute bias difference lower than -0.01 in 14 cases) and degradations (absolute bias difference greater than +0.01 in 21 cases) seen depending on PFTs and fluxes considered. The highest bias reductions are obtained for C4 grasses (GPP and TER), TemEBF (GPP and TER) and TemENF (GPP and TER); a degradation is observed for sensible heat flux over all PFTs.

For almost all variables and PFTs, accounting for the vegetation heterogeneity tends to improve the different metrics, but the magnitude of these improvements remains small, consistent with the high number of sites that retain the same agreement flag between both experiments (Fig. 6).

These results are consistent with other scoring metrics such as the Taylor Skill score (Taylor, 2001; Fig. S1) and a scoring following the approach of ILAMB (Collier et al., 2018; Fig. S2).

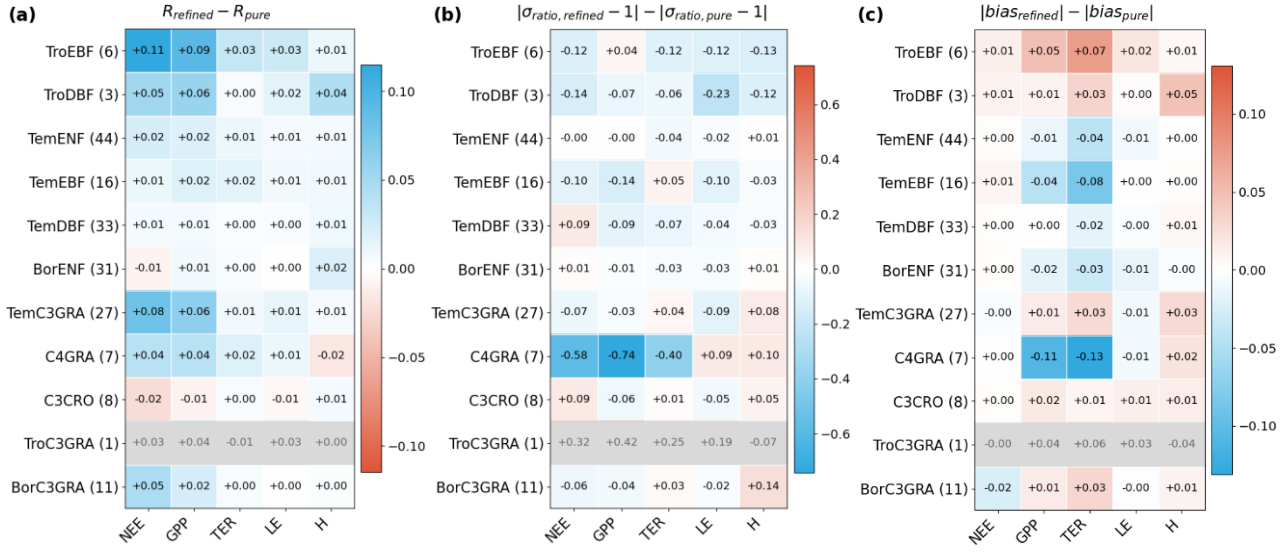


Figure 7: Differences (refined PFTs vs pure PFT) of (a) the correlation coefficient; (b) the variability ratio; (c) the absolute bias, per PFT (rows) and variable (columns). The statistics are computed on normalized time series. The blue color on the heatmap indicates that the refined PFTs led to enhanced

https://doi.org/10.5194/essd-2026-796
Preprint. Discussion started: 13 November 2026
© Author(s) 2026. CC BY 4.0 License.



model-data agreement. The number of sites in each PFT is written for each PFT label. If a PFT has less than 3 sites, the cells are grayed out.

4 Data availability

The database is available at the following DOI: https://doi.org/10.14768/6e99ff4b-3205-4038-8f9a-713e3e33753d (Tartaglione et al., 2026).

To support the database, we developed a publicly accessible website providing the refined PFT fractions for the different flux tower sites, and the associated information and flags detailed in Table 5. It features an interactive map to explore the database and to have facilitated access to the main information about each of the EC sites. This online tool provides the time series visualization in image format of the raw EC data and figures of ORCHIDEE simulations. The tool also provides the possibility to create and download files in the CSV format to get the desired metadata through several selection filters, such as vegetation type, etc.

The possibility to correct or discuss PFT fractions and other metadata is currently implemented as a GitLab ticket. This website is available at https://data.ipsl.fr/ecsitepftexplorer/index.html (last access: 25 September 2026) and a screenshot of the main page is shown in Fig. 8.

https://doi.org/10.5194/essd-2026-796
Preprint. Discussion started: 13 November 2026
© Author(s) 2026. CC BY 4.0 License.

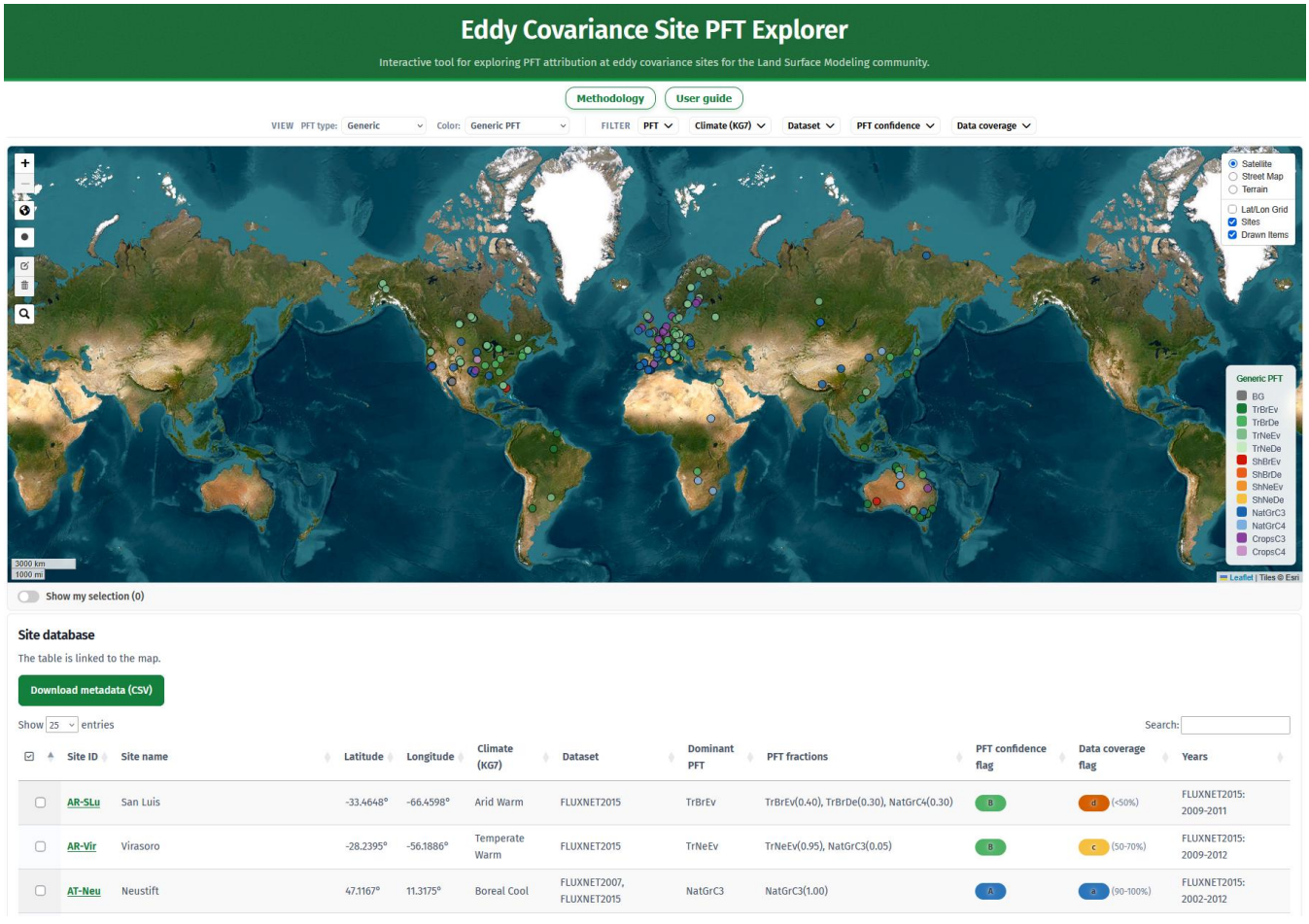


Figure 8: Snapshot of the website interface.

The eddy covariance data are available from the following datasets. The ICOS Warm Winter 2020 dataset at https://www.icos-cp.eu (Warm Winter 2020 Team, 2022): BE-Bra, BE-Dor, BE-Lon, BE-Vie, CH-Aws, CH-Cha, CH-Dav, CH-Fru, CH-Lae, CZ-BK1, CZ-KrP, CZ-Lnz, CZ-RAJ, CZ-Stn, DE-Geb, DE-Gri, DE-Hai, DE-HoH, DE-Hzd, DE-Kli, DE-Obe, DE-RuR, DE-RuS, DE-RuW, DE-Tha, DK-Sor, ES-Abr, ES-Agu, ES-LJu, ES-LM1, ES-LM2, FI-Hyy, FI-Ken, FI-Qvd, FI-Var, FR-Bil, FR-FBn, FR-Fon, FR-Gri, FR-Hes, FR-Tou, GF-Guy, IL-Yat, IT-BFt, IT-Cp2, IT-Lav, IT-MBo, IT-Ren, IT-SR2, IT-Tor, RU-Fy2, RU-Fyo, SE-Htm, SE-Nor, SE-Ros, SE-Svb. FLUXNET2015 dataset at https://fluxnet.org (Pastorello et al., 2020): AR-SLu, AR-Vir, AT-Neu, AU-Ade, AU-ASM, AU-Cpr, AU-Cum, AU-DaP, AU-DaS, AU-Dry,

https://doi.org/10.5194/essd-2026-796
Preprint. Discussion started: 13 November 2026
© Author(s) 2026. CC BY 4.0 License.


AU-Emr, AU-Gin, AU-GWW, AU-How, AU-Lox, AU-RDF, AU-Rig, AU-Rob, AU-Stp, AU-TTE, AU-Tum, AU-Wac, AU-Whr, AU-Wom, AU-Ync, BR-Sa3, CA-Man, CA-NS1, CA-NS2, CA-NS3, CA-NS4, CA-NS5, CA-NS6, CA-NS7, CA-Qfo, CA-SF1, CA-SF2, CA-SF3, CH-Oe1, CN-Cha, CN-Cng, CN-Dan, CN-Din, CN-Du2, CN-HaM, CN-Qia, CZ-BK2, DE-Lkb, DE-Seh, DK-Fou, ES-LgS, ES-Ln2, FI-Jok, FI-Sod, FR-LBr, FR-Pue, IT-CA2, IT-Col, IT-Cpz, IT-Isp, IT-La2, IT-Noe, IT-PT1, IT-Ro1, IT-Ro2, IT-SRo, JP-MBF, JP-SMF, NL-Loo, RU-Cok, RU-Ha1, SD-Dem, US-AR1, US-AR2, US-ARb, US-ARc, US-ARM, US-Blo, US-Cop, US-GLE, US-Ha1, US-KS2, US-Me2, US-Me6, US-MMS, US-Ne1, US-NR1, US-PFa, US-Prr, US-SRG, US-SRM, US-Syv, US-Ton, US-Tw3, US-UMB, US-UMd, US-Var, US-WCr, US-Whs, US-Wi0, US-Wi3, US-Wi4, US-Wi6, US-Wi9, US-Wkg, ZA-Kru, ZM-Mon. The AmeriFlux data at https://ameriflux.lbl.gov/: US-BZS, US-xBN, US-xDJ, US-xRM, US-xYE. The LaThuile data used in this study have an open-data use policy on the European Fluxes database (https://www.europe-fluxdata.eu): BE-Jal, BW-Ma1, DE-Bay, DE-Meh, DE-Wet, DK-Lva, DK-Ris, ES-ES1, ES-ES2, ES-LMa, ES-VDA, FR-Lq1, FR-Lq2, HU-Bug, HU-Mat, ID-Pag, IE-Ca1, IE-Dri, IT-Lec, IT-LMa, IT-Mal, IT-Non, IT-Pia, NL-Ca1, NL-Lan, NL-Lut, NL-Mol, PT-Esp, PT-Mi1, PT-Mi2, RU-Ha2, RU-Ha3, RU-Zot, SE-Fla, SE-Sk1, SE-Sk2, UK-EBu, UK-ESa, UK-Gri, UK-Ham, UK-Her, UK-PL3, UK-Tad, US-Aud, US-Bar, US-Bkg, US-FPe, US-Goo, US-Ho1, US-Ho2, US-Me4, US-MOz, US-Oho, US-SP1, US-SP2, US-WBW, US-Wi1, US-Wi2, US-Wi5, US-Wi7, US-Wi8. The individual citations can be found in table A1.

5. Discussion

5.1 Pertinence of the approach

The evaluation against the “pure” PFT approach demonstrates the validity of the approach for four (NEE, GPP, TER and LE) out of five fluxes. Problems remain with the sensible heat flux *H*, maybe in relation to the energy

https://doi.org/10.5194/essd-2026-796
Preprint. Discussion started: 13 November 2026
© Author(s) 2026. CC BY 4.0 License.


472 balance closure. While ORCHIDEE closes the energy budget at each time step, the energy fluxes data used in
473 the analysis are uncorrected, and the model-data error could therefore be explained by the imbalance more
474 than the PFT attribution. Further investigations, out of scope of this study, are needed to determine the
475 underlying cause of this particular behavior.
476 Beyond the comparison of the impact of using the attributed PFT fractions instead of a dominant PFT
477 approach, we provide three flags quantifying the confidence in the attributed PFT fractions, the completeness
478 of the measured fluxes and the model-data agreement. Along with the PFT fraction, these flags allow users
479 to select the best suited EC sites, depending on the purpose of their analysis: for example, a set of
480 homogeneous sites with a high data coverage (flags a-b), that the model already reproduces well (model-data
481 agreement 1-2). The traceable methodology we provide, together with remarks and sources supporting the
482 attribution, along with a quantification of the uncertainty (confidence flag), allows users to understand each
483 attribution, with the potential compromise we made, and to propose a revision through the associated
484 website if needed.

485 **5.2 Limitations of the study**

486 **5.2.1 Fixed footprint extents**

487 We adopted identical footprint extents for all the EC sites: a square of approximately 350 m (identify the close
488 vegetation contributing the most to the measurements) and a square of 1500 m (identify the distant
489 vegetation and vegetation heterogeneity), centered on the tower, rather than computing a specific footprint
490 for each site. The actual footprint size and shape vary with measurement height, wind direction, atmospheric
491 stability and vegetation type (Schmid, 2002; Kljun et al. 2015; Huang et al., 2022; Chu et al., 2021; Chu et al.,

https://doi.org/10.5194/essd-2026-796
Preprint. Discussion started: 13 November 2026
© Author(s) 2026. CC BY 4.0 License.


2026) and can range from a few tens of meters for short towers on grasslands to more than a kilometer for tall towers on adequate terrain. Using a flux footprint model, Fang et al. (2024) quantified the footprint area of 199 FLUXNET2015 sites, showing that the area contributing to 80% of the measured fluxes ranges from approximately 4000 m^2 to 7.3 km^2. They calculated a median of about 0.03 km^2 for grasslands and croplands and 2 km^2 for evergreen broadleaved forests. While our fixed extent approach encompasses most of the considered EC site's footprint, it can lead to the inclusion of vegetation type in the PFT fractions that contributes little to the measurements. Inversely, it could lead to the omission of vegetation that contributes and should be accounted for by the models. The last point may have a lower impact for LSMs simulations as the vegetation contribution to the measurements decrease with the distance from the flux tower.

5.2.2 Temporal variation of the vegetation

PFT fractions are assigned as static, but vegetation changes over time (land-use change, disturbances, management, etc.). EC measurements span several years during which vegetation may have changed, leading to different vegetation contributing to the measurements throughout the period, which should be reflected in LSM simulations. Hence a further enhancement would be to add a time dimension to the assigned PFT fractions.

5.2.3 Expert judgment

Although a majority of sites (58.5%) received the best confidence flag, the assignment of the PFT fractions relied partly on a subjective interpretation of the available information which can introduce non-reproducibility and potential inconsistency between sites. This limitation is mitigated by the presence of

https://doi.org/10.5194/essd-2026-796
Preprint. Discussion started: 13 November 2026
© Author(s) 2026. CC BY 4.0 License.


511 documented remarks highlighting the important information used for the assignment, and the possibility for
512 the community to propose revisions of the PFT fractions through the ticket system on the website.

513 **5.2.4 Data coverage flag and data cleaning approach**

514 The data coverage flag and the cleaning were based on our current ORCHIDEE formatting script that did not
515 include the fluxes quality check (QC) and only retained a binary meteorological quality check. A more detailed
516 QC would allow a more direct and representative data coverage flag and simplify the filtering. The formatting
517 ORCHIDEE script will be updated accordingly for the upcoming processing of the Shuttle database.
518 Nevertheless, the provider's QC may not capture all the targeted spurious data as the provider's flag reflects
519 the confidence of the gap-filling (based on three conditions) rather than the realism of the resulting values.

520 **6. Conclusions and perspectives**

521 We have presented a method to attribute PFT fractions to EC sites within a formal framework that minimises
522 subjective decisions and documents the information supporting the attributions.
523 The introduction of the three quality flags: the confidence flag reflecting our confidence in the attributed
524 PFTs, the data coverage flag reflecting the completeness of the measurements based on our cleaning
525 approach, and the model-data agreement flag, based on prior simulations with the ORCHIDEE LSM. These
526 flags give a rapid overview of the data quality and model performance at each EC site.
527 We compared the impact of a PFT fractions representation against a single, dominant PFT approach, on
528 ORCHIDEE simulations, that showed positive results for four out of five fluxes studied demonstrating the
529 pertinence of the approach.

https://doi.org/10.5194/essd-2026-796
Preprint. Discussion started: 13 November 2026
© Author(s) 2026. CC BY 4.0 License.


This work led to the production of a publicly available database and its associated website that allows to explore 229 EC sites, their supporting information and visualisation of the fluxes time series.

Recent initiatives have been developed to gather and synthesize site-level information, such as the flux tower site attribute dataset for LSMs of Shi et al. (2025) and also interactive tools such as the FLUXNET Data Explorer (Keenan, 2026; https://www.keenangroup.info/fluxnet-data-explorer/, last access: 21 June 2026) that provides access to the catalog of the FLUXNET Shuttle, the Observatoire des Flux (https://observatoire-des-flux.inrae.fr/, last access: 24 June 2026) that documents the EC sites of the INRAE network, with metadata, imagery and time series visualization. These initiatives are likely to expand with the large number of new EC sites and new site-years arriving in a continuous flow with the FLUXNET Shuttle. However there is still a gap of information that LSMs require: the characterization of the vegetation spatial heterogeneity and the description of the vegetation in terms of PFTs, directly usable by models. This work aimed to solve this gap.

The attribution of the PFTs relied on publicly available information. We anticipate that the website will facilitate the consultation of the PI, allowing them to review and if needed, correct the information allowing the PFT attribution.

Several extensions of this work are possible. The static approach could be replaced by a time-varying vegetation cover and the fixed extents could be replaced by site's specific footprint, accounting for a finer representation of the contributing vegetation in the EC measurements. The model-data agreement flag, for the moment only computed with the ORCHIDEE LSM, could be extended to other LSMs and integrated with tools such as https://modelevaluation.org (last access: 21 June 2026) that intend to perform model evaluation and benchmarking.

https://doi.org/10.5194/essd-2026-796
Preprint. Discussion started: 13 November 2026
© Author(s) 2026. CC BY 4.0 License.



The most valuable outcome for this work would be its integration into such existing tools and its maintenance by the FLUXNET and the LSM communities, so that a consistent PFT information usable by LSMs becomes a standard part of the information available for EC sites.

Acknowledgments

This study has been made in the context of the CORSO project (grant agreement No. 101082194). FM and CB were also supported by the CNES-TOSCA FORGE project, and the ANR FACET project (grant number ANR-23-CE01-0016).

We thank the ORCHIDEE group for developing and maintaining the code. We thank Xiaoni Wang-Faivre for the attribution of the PLUMBER2 ORCHIDEE PFT fractions. We thank the IT team of LSCE for their continuous support.

VT used generative AI for help with the python scripts and to develop the associated website.

Author contribution

Vincent Tartaglione: Conceptualization, data curation, formal analysis, investigation, methodology, software, validation, visualization, writing (original draft preparation), writing (review and editing); **Fabienne Maignan:** Conceptualization, data curation, formal analysis, funding acquisition, investigation, methodology, project administration, software, supervision, validation, visualization, writing (original draft preparation), writing (review and editing); **Philippe Peylin:** Funding acquisition, supervision, writing (review and editing); **Vladislav Bastrikov:** Data curation, methodology, software; **Cédric Bacour:** Conceptualization, data curation, formal analysis, investigation, methodology, project administration, software, supervision, validation, visualization, writing (original draft preparation), writing (review and editing).

https://doi.org/10.5194/essd-2026-796
Preprint. Discussion started: 13 November 2026
© Author(s) 2026. CC BY 4.0 License.



References

Abadie, C., Maignan, F., Remaud, M., Kohonen, K., Sun, W., Kooijmans, L., Vesala, T., Seibt, U., Raoult, N., Bastrikov, V., Belviso, S., and Peylin, P.: Carbon and Water Fluxes of the Boreal Evergreen Needleleaf Forest Biome Constrained by Assimilating Ecosystem Carbonyl Sulfide Flux Observations, JGR Biogeosciences, 128, e2023JG007407, https://doi.org/10.1029/2023JG007407, 2023.

Abramowitz, G., Ukkola, A., Hobeichi, S., Cranko Page, J., Lipson, M., De Kauwe, M. G., Green, S., Brenner, C., Frame, J., Nearing, G., Clark, M., Best, M., Anthoni, P., Arduini, G., Boussetta, S., Caldararu, S., Cho, K., Cuntz, M., Fairbairn, D., Ferguson, C. R., Kim, H., Kim, Y., Knauer, J., Lawrence, D., Luo, X., Malyshev, S., Nitta, T., Ogee, J., Oleson, K., Ottlé, C., Peylin, P., De Rosnay, P., Rumbold, H., Su, B., Vuichard, N., Walker, A. P., Wang-Faivre, X., Wang, Y., and Zeng, Y.: On the predictability of turbulent fluxes from land: PLUMBER2 MIP experimental description and preliminary results, Biogeosciences, 21, 5517–5538, https://doi.org/10.5194/bg-21-5517-2024, 2024.

Acosta, M., Czerný, R., Fischer, M., ICOS Ecosystem Thematic Centre, and Trotta, C.: Warm winter 2020 ecosystem eddy covariance flux product from Kresin u Pacova (1.0), https://doi.org/10.18160/9A8S-EJVK, 2022.

Amiro, B.: FLUXNET2015 CA-Man Manitoba - Northern Old Black Spruce (former BOREAS Northern Study Area), https://doi.org/10.18140/FLX/1440035, 2016a.

Amiro, B.: FLUXNET2015 CA-SF1 Saskatchewan - Western Boreal, forest burned in 1977, https://doi.org/10.18140/FLX/1440046, 2016b.

Amiro, B.: FLUXNET2015 CA-SF2 Saskatchewan - Western Boreal, forest burned in 1989, https://doi.org/10.18140/FLX/1440047, 2016c.

Amiro, B.: FLUXNET2015 CA-SF3 Saskatchewan - Western Boreal, forest burned in 1998, https://doi.org/10.18140/FLX/1440048, 2016d.

Ammann, C.: FLUXNET2015 CH-Oe1 Oensingen grassland, https://doi.org/10.18140/FLX/1440135, 2016.

https://doi.org/10.5194/essd-2026-796
Preprint. Discussion started: 13 November 2026
© Author(s) 2026. CC BY 4.0 License.



595 Ardö, J., El Tahir, B. A., and ElKhidir, H. A. M.: FLUXNET2015 SD-Dem Demokeya,
596 https://doi.org/10.18140/FLX/1440186, 2016.

597 Arndt, S., Hinko-Najera, N., and Griebel, A.: FLUXNET2015 AU-Wom Wombat,
598 https://doi.org/10.18140/FLX/1440207, 2016.

599 Arriga, N., Goded, I., Manca, G., ICOS Ecosystem Thematic Centre, and Trotta, C.: Warm winter 2020 ecosystem
600 eddy covariance flux product from San Rossore 2 (1.0), https://doi.org/10.18160/EPYB-PSFM, 2022.

601 Aurela, M., Tuovinen, J.-P., Hatakka, J., Lohila, A., Mäkelä, T., Rainne, J., and Lauria, T.: FLUXNET2015 FI-Sod
602 Sodankyla, https://doi.org/10.18140/FLX/1440160, 2016.

603 Aurela, M., Laurila, T., Lohila, A., ICOS Ecosystem Thematic Centre, and Trotta, C.: Warm winter 2020
604 ecosystem eddy covariance flux product from Kenttarova (1.0), https://doi.org/10.18160/W8QV-2Z04, 2022.

605 Bacour, C., MacBean, N., Chevallier, F., Léonard, S., Koffi, E. N., and Peylin, P.: Assimilation of multiple datasets
606 results in large differences in regional- to global-scale NEE and GPP budgets simulated by a terrestrial
607 biosphere model, Biogeosciences, 20, 1089–1111, https://doi.org/10.5194/bg-20-1089-2023, 2023.

608 Baldocchi, D. and Ma, S.: FLUXNET2015 US-Ton Tonzi Ranch, https://doi.org/10.18140/FLX/1440092, 2016.

609 Baldocchi, D., Falge, E., Gu, L., Olson, R., Hollinger, D., Running, S., Anthoni, P., Bernhofer, C., Davis, K., Evans,
610 R., Fuentes, J., Goldstein, A., Katul, G., Law, B., Lee, X., Malhi, Y., Meyers, T., Munger, W., Oechel, W., Paw, K. T.,
611 Pilegaard, K., Schmid, H. P., Valentini, R., Verma, S., Vesala, T., Wilson, K., and Wofsy, S.: FLUXNET: A New Tool
612 to Study the Temporal and Spatial Variability of Ecosystem–Scale Carbon Dioxide, Water Vapor, and Energy
613 Flux Densities, Bull. Amer. Meteor. Soc., 82, 2415–2434, https://doi.org/10.1175/1520-
614 0477(2001)082<2415:FANTTS>2.3.CO;2, 2001.

615 Baldocchi, D., Ma, S., and Xu, L.: FLUXNET2015 US-Var Vaira Ranch- Ione,
616 https://doi.org/10.18140/FLX/1440094, 2016.

617 Bastrikov, V., MacBean, N., Bacour, C., Santaren, D., Kuppel, S., and Peylin, P.: Land surface model parameter
618 optimisation using in situ flux data: comparison of gradient-based versus random search algorithms (a case
619 study using ORCHIDEE v1.9.5.2), Geosci. Model Dev., 11, 4739–4754, https://doi.org/10.5194/gmd-11-4739-
620 2018, 2018.

https://doi.org/10.5194/essd-2026-796
Preprint. Discussion started: 13 November 2026
© Author(s) 2026. CC BY 4.0 License.

Belelli, L., Papale, D., and Valentini, R.: FLUXNET2015 RU-Ha1 Hakasia steppe, https://doi.org/10.18140/FLX/1440184, 2016.

Berbigier, P. and Loustau, D.: FLUXNET2015 FR-LBr Le Bray, https://doi.org/10.18140/FLX/1440163, 2016.

Beringer, J. and Hutley, L.: FLUXNET2015 AU-Ade Adelaide River, https://doi.org/10.18140/FLX/1440193, 2016a.

Beringer, J. and Hutley, L.: FLUXNET2015 AU-DaP Daly River Savanna, https://doi.org/10.18140/FLX/1440123, 2016b.

Beringer, J. and Hutley, L.: FLUXNET2015 AU-Dry Dry River, https://doi.org/10.18140/FLX/1440197, 2016c.

Beringer, J. and Hutley, L.: FLUXNET2015 AU-How Howard Springs, https://doi.org/10.18140/FLX/1440125, 2016d.

Beringer, J. and Hutley, L.: FLUXNET2015 AU-RDF Red Dirt Melon Farm, Northern Territory, https://doi.org/10.18140/FLX/1440201, 2016e.

Beringer, J. and Hutley, L.: FLUXNET2015 AU-Stp Sturt Plains, https://doi.org/10.18140/FLX/1440204, 2016f.

Beringer, J. and Hutley, P. L.: FLUXNET2015 AU-DaS Daly River Cleared, https://doi.org/10.18140/FLX/1440122, 2016g.

Beringer, J. and Walker, J.: FLUXNET2015 AU-Ync Jaxa, https://doi.org/10.18140/FLX/1440208, 2016.

Beringer, J., Cunningham, S., Baker, P., Cavagnaro, T., MacNally, R., Thompson, R., and McHugh, I.: FLUXNET2015 AU-Rig Riggs Creek, https://doi.org/10.18140/FLX/1440202, 2016a.

Beringer, J., Hutley, L., McGuire, D., and U, P.: FLUXNET2015 AU-Wac Wallaby Creek, https://doi.org/10.18140/FLX/1440127, 2016b.

Beringer, J., Cunningham, S., Baker, P., Cavagnaro, T., MacNally, R., Thompson, R., and McHugh, I.: FLUXNET2015 AU-Whr Whroo, https://doi.org/10.18140/FLX/1440206, 2016c.

https://doi.org/10.5194/essd-2026-796
Preprint. Discussion started: 13 November 2026
© Author(s) 2026. CC BY 4.0 License.

Bernhofer, C., Gruenwald, J. T., ICOS Ecosystem Thematic Centre, and Trotta, C.: Warm winter 2020 ecosystem eddy covariance flux product from Grillenburg (1.0), https://doi.org/10.18160/A4NW-3VE1, 2022a.

Bernhofer, C., Gruenwald, J. T., ICOS Ecosystem Thematic Centre, and Trotta, C.: Warm winter 2020 ecosystem eddy covariance flux product from Hetzdorf (1.0), https://doi.org/10.18160/GBJS-Y2FT, 2022b.

Bernhofer, C., Gruenwald, J. T., ICOS Ecosystem Thematic Centre, and Trotta, C.: Warm winter 2020 ecosystem eddy covariance flux product from Klingenberg (1.0), https://doi.org/10.18160/76VR-FWJ6, 2022c.

Bernhofer, C., Gruenwald, J. T., ICOS Ecosystem Thematic Centre, and Trotta, C.: Warm winter 2020 ecosystem eddy covariance flux product from Oberbärenburg (1.0), https://doi.org/10.18160/05Y0-QP67, 2022d.

Bernhofer, C., Gruenwald, J. T., ICOS Ecosystem Thematic Centre, and Trotta, C.: Warm winter 2020 ecosystem eddy covariance flux product from Tharandt (1.0), https://doi.org/10.18160/8FBV-1K18, 2022e.

Best, M. J., Pryor, M., Clark, D. B., Rooney, G. G., Essery, R. . L. H., Ménard, C. B., Edwards, J. M., Hendry, M. A., Porson, A., Gedney, N., Mercado, L. M., Sitch, S., Blyth, E., Boucher, O., Cox, P. M., Grimmond, C. S. B., and Harding, R. J.: The Joint UK Land Environment Simulator (JULES), model description – Part 1: Energy and water fluxes, Geosci. Model Dev., 4, 677–699, https://doi.org/10.5194/gmd-4-677-2011, 2011.

Billesbach, D., Bradford, J., and Torn, M.: FLUXNET2015 US-AR1 ARM USDA UNL OSU Woodward Switchgrass 1, https://doi.org/10.18140/FLX/1440103, 2016a.

Billesbach, D., Bradford, J., and Torn, M.: FLUXNET2015 US-AR2 ARM USDA UNL OSU Woodward Switchgrass 2, https://doi.org/10.18140/FLX/1440104, 2016b.

Biraud, S., Fischer, M., Chan, S., and Torn, M.: FLUXNET2015 US-ARM ARM Southern Great Plains site- Lamont, https://doi.org/10.18140/FLX/1440066, 2016.

Blanken, P. D., Monson, R. K., Burns, S. P., Bowling, D. R., and Turnipseed, A. A.: FLUXNET2015 US-NR1 Niwot Ridge Forest (LTER NWT1), https://doi.org/10.18140/FLX/1440087, 2016.

Bonal, D., Burban, B., ICOS Ecosystem Thematic Centre, and Trotta, C.: Warm winter 2020 ecosystem eddy covariance flux product from Guyaflux (1.0), https://doi.org/10.18160/BMST-X8NQ, 2022.

https://doi.org/10.5194/essd-2026-796
Preprint. Discussion started: 13 November 2026
© Author(s) 2026. CC BY 4.0 License.



667 Botta, A., Viovy, N., Ciais, P., Friedlingstein, P., and Monfray, P.: A global prognostic scheme of leaf onset using
668 satellite data, Global Change Biology, 6, 709–725, https://doi.org/10.1046/j.1365-2486.2000.00362.x, 2000.

669 Boucher, O., Servonnat, J., Albright, A. L., Aumont, O., Balkanski, Y., Bastrikov, V., Bekki, S., Bonnet, R., Bony,
670 S., Bopp, L., Braconnot, P., Brockmann, P., Cadule, P., Caubel, A., Cheruy, F., Codron, F., Cozic, A., Cugnet, D.,
671 D'Andrea, F., Davini, P., De Lavergne, C., Denvil, S., Deshayes, J., Devilliers, M., Ducharne, A., Dufresne, J.,
672 Dupont, E., Éthé, C., Fairhead, L., Falletti, L., Flavoni, S., Foujols, M., Gardoll, S., Gastineau, G., Ghattas, J.,
673 Grandpeix, J., Guenet, B., Guez, L., E., Guilyardi, E., Guimberteau, M., Hauglustaine, D., Hourdin, F., Idelkadi,
674 A., Joussaume, S., Kageyama, M., Khodri, M., Krinner, G., Lebas, N., Levavasseur, G., Lévy, C., Li, L., Lott, F.,
675 Lurton, T., Luyssaert, S., Madec, G., Madeleine, J., Maignan, F., Marchand, M., Marti, O., Mellul, L., Meurdesoif,
676 Y., Mignot, J., Musat, I., Ottlé, C., Peylin, P., Planton, Y., Polcher, J., Rio, C., Rochetin, N., Rousset, C., Sepulchre,
677 P., Sima, A., Swingedouw, D., Thiéblemont, R., Traore, A. K., Vancoppenolle, M., Vial, J., Vialard, J., Viovy, N., and
678 Vuichard, N.: Presentation and Evaluation of the IPSL-CM6A-LR Climate Model, J Adv Model Earth Syst, 12,
679 e2019MS002010, https://doi.org/10.1029/2019MS002010, 2020.

680 Bowling, D.: FLUXNET2015 US-Cop Corral Pocket, https://doi.org/10.18140/FLX/1440100, 2016.

681 Bruemmer, C., Schrader, F., Delorme, J.-P., Lucas-Moffat, A., ICOS Ecosystem Thematic Centre, and Trotta, C.:
682 Warm winter 2020 ecosystem eddy covariance flux product from Gebesee (1.0),
683 https://doi.org/10.18160/KVAC-KYEX, 2022.

684 Buchmann, N., Eugster, W., Ghiasi, S., ICOS Ecosystem Thematic Centre, and Trotta, C.: Warm winter 2020
685 ecosystem eddy covariance flux product from Alp Weissenstein (1.0), https://doi.org/10.18160/ASYZ-4T3X,
686 2022a.

687 Buchmann, N., Merbold, L., Fuchs, K., Feigenwinter, I., ICOS Ecosystem Thematic Centre, and Trotta, C.: Warm
688 winter 2020 ecosystem eddy covariance flux product from Chamau grassland (1.0),
689 https://doi.org/10.18160/V5RX-VAWY, 2022b.

690 Buchmann, N., Hörtnagl, L., Merbold, L., Gharun, M., ICOS Ecosystem Thematic Centre, and Trotta, C.: Warm
691 winter 2020 ecosystem eddy covariance flux product from Davos (1.0), https://doi.org/10.18160/1JA9-VJEV,
692 2022c.

© Author(s) 2026. CC BY 4.0 License.

Buchmann, N., Eugster, W., Hörtnagl, L., Fuchs, K., ICOS Ecosystem Thematic Centre, and Trotta, C.: Warm winter 2020 ecosystem eddy covariance flux product from Fruebuel grassland (1.0), https://doi.org/10.18160/4SAX-0ZYA, 2022d.

Buchmann, N., Eugster, W., Paul-Limoges, E., Gharun, M., ICOS Ecosystem Thematic Centre, and Trotta, C.: Warm winter 2020 ecosystem eddy covariance flux product from Laegern (1.0), https://doi.org/10.18160/51Z6-S5XF, 2022e.

C3S: ERA5 hourly data on single levels from 1940 to present, https://doi.org/10.24381/CDS.ADBB2D47, 2018.

Calvet, J.-C., ICOS Ecosystem Thematic Centre, and Trotta, C.: Warm winter 2020 ecosystem eddy covariance flux product from Toulouse (1.0), https://doi.org/10.18160/6KQG-97TD, 2022.

Cescatti, A., Marcolla, B., Zorer, R., and Gianelle, D.: FLUXNET2015 IT-La2 Lavarone2, https://doi.org/10.18140/FLX/1440235, 2016.

Chen, J.: FLUXNET2015 US-Wi0 Young red pine (YRP), https://doi.org/10.18140/FLX/1440055, 2016a.

Chen, J.: FLUXNET2015 US-Wi3 Mature hardwood (MHW), https://doi.org/10.18140/FLX/1440057, 2016b.

Chen, J.: FLUXNET2015 US-Wi4 Mature red pine (MRP), https://doi.org/10.18140/FLX/1440058, 2016c.

Chen, J.: FLUXNET2015 US-Wi6 Pine barrens #1 (PB1), https://doi.org/10.18140/FLX/1440060, 2016d.

Chen, J.: FLUXNET2015 US-Wi9 Young Jack pine (YJP), https://doi.org/10.18140/FLX/1440063, 2016e.

Chen, L., Dirmeyer, P. A., Guo, Z., and Schultz, N. M.: Pairing FLUXNET sites to validate model representations of land-use/land-cover change, Hydrol. Earth Syst. Sci., 22, 111–125, https://doi.org/10.5194/hess-22-111-2018, 2018.

Chen, S.: FLUXNET2015 CN-Du2 Duolun_grassland (D01), https://doi.org/10.18140/FLX/1440140, 2016f.

Chini, L., Hurtt, G., Sahajpal, R., Frolking, S., Klein Goldewijk, K., Sitch, S., Ganzenmüller, R., Ma, L., Ott, L., Pongratz, J., and Poulter, B.: Land-use harmonization datasets for annual global carbon budgets, Earth Syst. Sci. Data, 13, 4175–4189, https://doi.org/10.5194/essd-13-4175-2021, 2021.

https://doi.org/10.5194/essd-2026-796
Preprint. Discussion started: 13 November 2026
© Author(s) 2026. CC BY 4.0 License.



716 Chu, H., Luo, X., Ouyang, Z., Chan, W. S., Dengel, S., Biraud, S. C., Torn, M. S., Metzger, S., Kumar, J., Arain, M.
717 A., Arkebauer, T. J., Baldocchi, D., Bernacchi, C., Billesbach, D., Black, T. A., Blanken, P. D., Bohrer, G., Bracho,
718 R., Brown, S., Brunsell, N. A., Chen, J., Chen, X., Clark, K., Desai, A. R., Duman, T., Durden, D., Fares, S., Forbrich,
719 I., Gamon, J. A., Gough, C. M., Griffis, T., Helbig, M., Hollinger, D., Humphreys, E., Ikawa, H., Iwata, H., Ju, Y.,
720 Knowles, J. F., Knox, S. H., Kobayashi, H., Kolb, T., Law, B., Lee, X., Litvak, M., Liu, H., Munger, J. W., Noormets,
721 A., Novick, K., Oberbauer, S. F., Oechel, W., Oikawa, P., Papuga, S. A., Pendall, E., Prajapati, P., Prueger, J.,
722 Quinton, W. L., Richardson, A. D., Russell, E. S., Scott, R. L., Starr, G., Staebler, R., Stoy, P. C., Stuart-Haëntjens,
723 E., Sonnentag, O., Sullivan, R. C., Suyker, A., Ueyama, M., Vargas, R., Wood, J. D., and Zona, D.:
724 Representativeness of Eddy-Covariance flux footprints for areas surrounding AmeriFlux sites, Agricultural
725 and Forest Meteorology, 301–302, 108350, https://doi.org/10.1016/j.agrformet.2021.108350, 2021.

726 Chu, H., Metzger, S., Ouyang, Z., Griebel, A., Yi, K., Durden, D., Wolf, S., Kasak, K., Rey-Sanchez, C., Hernandez
727 Rodriguez, L. C., Oikawa, P., Falco, N., Runkle, B. R. K., Ahmadi, A., and Matthes, J.: Flux Footprints: A Critical
728 Link to Bridge Eddy-Covariance Measurements With Models, Remote Sensing, and Other Observations,
729 Global Change Biology, 32, e70887, https://doi.org/10.1111/gcb.70887, 2026.

730 Clark, D. B., Mercado, L. M., Sitch, S., Jones, C. D., Gedney, N., Best, M. J., Pryor, M., Rooney, G. G., Essery, R. L.
731 H., Blyth, E., Boucher, O., Harding, R. J., Huntingford, C., and Cox, P. M.: The Joint UK Land Environment
732 Simulator (JULES), model description – Part 2: Carbon fluxes and vegetation dynamics, Geosci. Model Dev., 4,
733 701–722, https://doi.org/10.5194/gmd-4-701-2011, 2011.

734 Cleverly, J. and Eamus, D.: FLUXNET2015 AU-ASM Alice Springs, https://doi.org/10.18140/FLX/1440194, 2016a.

735 Cleverly, J. and Eamus, D.: FLUXNET2015 AU-TTE Ti Tree East, https://doi.org/10.18140/FLX/1440205, 2016b.

736 Collier, N., Hoffman, F. M., Lawrence, D. M., Keppel-Aleks, G., Koven, C. D., Riley, W. J., Mu, M., and Randerson,
737 J. T.: The International Land Model Benchmarking (ILAMB) System: Design, Theory, and Implementation, J Adv
738 Model Earth Syst, 10, 2731–2754, https://doi.org/10.1029/2018MS001354, 2018.

739 Copernicus Climate Change Service: ERA-Interim atmospheric reanalysis,
740 https://doi.org/10.24381/CDS.F2F5241D, 2023.

https://doi.org/10.5194/essd-2026-796
Preprint. Discussion started: 13 November 2026
© Author(s) 2026. CC BY 4.0 License.



741 Cremonese, E., Galvagno, M., Morra di Cella, U., Migliavacca, M., ICOS Ecosystem Thematic Centre, and Trotta,
742 C.: Warm winter 2020 ecosystem eddy covariance flux product from Torgnon (1.0),
743 https://doi.org/10.18160/9J7C-Q5QP, 2022.

744 Cuntz, M., Longdoz, B., ICOS Ecosystem Thematic Centre, and Trotta, C.: Warm winter 2020 ecosystem eddy
745 covariance flux product from Hesse (1.0), https://doi.org/10.18160/GFQX-22T7, 2022.

746 Desai, A.: FLUXNET2015 US-PFa Park Falls/WLEF, https://doi.org/10.18140/FLX/1440089, 2016a.

747 Desai, A.: FLUXNET2015 US-Syv Sylvania Wilderness Area, https://doi.org/10.18140/FLX/1440091, 2016b.

748 Desai, A.: FLUXNET2015 US-WCr Willow Creek, https://doi.org/10.18140/FLX/1440095, 2016c.

749 Di Gregorio, A. and Jansen, L. J. M. (Eds.): Land cover classification system (LCCS): classification concepts and
750 user manual; for software version 1.0, Repr., FAO, Rome, 179 pp., ISBN 978-92-5-104216-8,
751 https://www.fao.org/4/x0596e/x0596e00.htm (last access: 09 October 2026), 2001.

752 Dolman, H., Van Der Molen, M., Parmentier, F.-J., Marchesini, L. B., Dean, J., Van Huissteden, K., and Maximov,
753 T.: FLUXNET2015 RU-Cok Chokurdakh, https://doi.org/10.18140/FLX/1440182, 2016.

754 Dong, G.: FLUXNET2015 CN-Cng Changling, https://doi.org/10.18140/FLX/1440209, 2016.

755 Drake, B. and Hinkle, R.: FLUXNET2015 US-KS2 Kennedy Space Center (scrub oak),
756 https://doi.org/10.18140/FLX/1440075, 2016.

757 Dufrêne, E., Berveiller, D., Delpierre, N., ICOS Ecosystem Thematic Centre, and Trotta, C.: Warm winter 2020
758 ecosystem eddy covariance flux product from Fontainebleau-Barbeau (1.0), https://doi.org/10.18160/X1J0-
759 H684, 2022.

760 El-Madany, T. S., Migliavacca, M., Carrara, A., Reichstein, M., ICOS Ecosystem Thematic Centre, and Trotta, C.:
761 Warm winter 2020 ecosystem eddy covariance flux product from Albuera (1.0),
762 https://doi.org/10.18160/BWYS-J050, 2022a.

763 El-Madany, T. S., Migliavacca, M., Carrara, A., Reichstein, M., ICOS Ecosystem Thematic Centre, and Trotta, C.:
764 Warm winter 2020 ecosystem eddy covariance flux product from Majadas del Tietar South (1.0),
765 https://doi.org/10.18160/G6H4-6AY6, 2022b.

https://doi.org/10.5194/essd-2026-796
Preprint. Discussion started: 13 November 2026
© Author(s) 2026. CC BY 4.0 License.

Euskirchen, E.: AmeriFlux FLUXNET-1F US-BZS Bonanza Creek Black Spruce, https://doi.org/10.17190/AMF/1881572, 2022.

ESA. Land Cover CCI Product User Guide Version 2. Tech. Rep., https://maps.elie.ucl.ac.be/CCI/viewer/download/ESACCI-LC-Ph2-PUGv2_2.0.pdf (last access: 09 October 2026), 2017.

Ewenz, C., Stevens, R., and Grigson, G.: FLUXNET2015 AU-Lox Loxton, https://doi.org/10.18140/FLX/1440247, 2016.

Fang, J., Fang, J., Chen, B., Zhang, H., Dilawar, A., Guo, M., and Liu, S.: Assessing Spatial Representativeness of Global Flux Tower Eddy-Covariance Measurements Using Data from FLUXNET2015, Sci Data, 11, 569, https://doi.org/10.1038/s41597-024-03291-3, 2024.

Fares, S., Conte, A., ICOS Ecosystem Thematic Centre, and Trotta, C.: Warm winter 2020 ecosystem eddy covariance flux product from Castelporziano2 (1.0), https://doi.org/10.18160/WSAC-6XY6, 2022.

Garcia, A., Di Bella, C., Houspanossian, J., Magliano, P., Jobbágy, E., Posse, G., Fernández, R., and Nosetto, M.: FLUXNET2015 AR-SLu San Luis, https://doi.org/10.18140/FLX/1440191, 2016.

Gerosa, G., Finco, A., Marzuoli, R., Chiesa, M., ICOS Ecosystem Thematic Centre, and Trotta, C.: Warm winter 2020 ecosystem eddy covariance flux product from Bosco Fontana (1.0), https://doi.org/10.18160/M6XJ-Q0B3, 2022.

Gianelle, D., Belelli Marchesini, L., Sottocornola, M., ICOS Ecosystem Thematic Centre, and Trotta, C.: Warm winter 2020 ecosystem eddy covariance flux product from Lavarone (1.0), https://doi.org/10.18160/HZSQ-G19C, 2022a.

Gianelle, D., Belelli Marchesini, L., Marcolla, B., Sottocornola, M., ICOS Ecosystem Thematic Centre, and Trotta, C.: Warm winter 2020 ecosystem eddy covariance flux product from Monte Bondone (1.0), https://doi.org/10.18160/G9KE-399C, 2022b.

Goldstein, A.: FLUXNET2015 US-Blo Blodgett Forest, https://doi.org/10.18140/FLX/1440068, 2016.

https://doi.org/10.5194/essd-2026-796
Preprint. Discussion started: 13 November 2026
© Author(s) 2026. CC BY 4.0 License.



790 Gough, C., Bohrer, G., and Curtis, P.: FLUXNET2015 US-UMB Univ. of Mich. Biological Station,
791 https://doi.org/10.18140/FLX/1440093, 2016a.

792 Gough, C., Bohrer, G., and Curtis, P.: FLUXNET2015 US-UMd UMBS Disturbance,
793 https://doi.org/10.18140/FLX/1440101, 2016b.

794 Goulden, M.: FLUXNET2015 BR-Sa3 Santarem-Km83-Logged Forest, https://doi.org/10.18140/FLX/1440033,
795 2016a.

796 Goulden, M.: FLUXNET2015 CA-NS1 UCI-1850 burn site, https://doi.org/10.18140/FLX/1440036, 2016b.

797 Goulden, M.: FLUXNET2015 CA-NS2 UCI-1930 burn site, https://doi.org/10.18140/FLX/1440037, 2016c.

798 Goulden, M.: FLUXNET2015 CA-NS3 UCI-1964 burn site, https://doi.org/10.18140/FLX/1440038, 2016d.

799 Goulden, M.: FLUXNET2015 CA-NS4 UCI-1964 burn site wet, https://doi.org/10.18140/FLX/1440039, 2016e.

800 Goulden, M.: FLUXNET2015 CA-NS5 UCI-1981 burn site, https://doi.org/10.18140/FLX/1440040, 2016f.

801 Goulden, M.: FLUXNET2015 CA-NS6 UCI-1989 burn site, https://doi.org/10.18140/FLX/1440041, 2016g.

802 Goulden, M.: FLUXNET2015 CA-NS7 UCI-1998 burn site, https://doi.org/10.18140/FLX/1440042, 2016h.

803 Gruening, C., Goded, I., Cescatti, A., and Pokorska, O.: FLUXNET2015 IT-Isp Ispra ABC-IS,
804 https://doi.org/10.18140/FLX/1440234, 2016a.

805 Gruening, C., Goded, I., Cescatti, A., Manca, G., and Seufert, G.: FLUXNET2015 IT-SRo San Rossore,
806 https://doi.org/10.18140/FLX/1440176, 2016b.

807 Harper, K. L., Lamarche, C., Hartley, A., Peylin, P., Ottlé, C., Bastrikov, V., San Martín, R., Bohnenstengel, S. I.,
808 Kirches, G., Boettcher, M., Shevchuk, R., Brockmann, C., and Defourny, P.: A 29-year time series of annual 300
809 m resolution plant-functional-type maps for climate models, Earth Syst. Sci. Data, 15, 1465–1499,
810 https://doi.org/10.5194/essd-15-1465-2023, 2023a.

811 Harper, K. L., Lamarche, C., Hartley, A., Peylin, P., Ottlé, C., Bastrikov, V., San Martín, R., Bohnenstengel, S. I.,
812 Kirches, G., Boettcher, M., Shevchuk, R., Brockmann, C., and Defourny, P.: ESA Land Cover Climate Change

© Author(s) 2026. CC BY 4.0 License.



Initiative (Land_Cover_cci): Global Plant Functional Types (PFT) Dataset, v2.0.8, https://doi.org/10.5285/26A0F46C95EE4C29B5C650B129AAB788, 2023b.

Hartley, A. J., MacBean, N., Georgievski, G., and Bontemps, S.: Uncertainty in plant functional type distributions and its impact on land surface models, Remote Sensing of Environment, 203, 71–89, https://doi.org/10.1016/j.rse.2017.07.037, 2017.

Heimsch, L., Lohila, A., Kulmala, L., ICOS Ecosystem Thematic Centre, and Trotta, C.: Warm winter 2020 ecosystem eddy covariance flux product from Qvidja (1.0), https://doi.org/10.18160/T08C-4J0P, 2022.

Heinesch, B., De Ligne, A., de la Motte, L. G., Manise, T., ICOS Ecosystem Thematic Centre, and Trotta, C.: Warm winter 2020 ecosystem eddy covariance flux product from Dorinne (1.0), https://doi.org/10.18160/P7JG-DVR4, 2022a.

Heinesch, B., De Ligne, A., Manise, T., Longdoz, B., ICOS Ecosystem Thematic Centre, and Trotta, C.: Warm winter 2020 ecosystem eddy covariance flux product from Lonzee (1.0), https://doi.org/10.18160/46P3-WT1D, 2022b.

Heliasz, M., Holst, J., ICOS Ecosystem Thematic Centre, and Trotta, C.: Warm winter 2020 ecosystem eddy covariance flux product from Hyltemossa (1.0), https://doi.org/10.18160/HQJA-PCXX, 2022.

Huang, X., Lin, S., Li, X., Ma, M., Wu, C., and Yuan, W.: How Well Can Matching High Spatial Resolution Landsat Data with Flux Tower Footprints Improve Estimates of Vegetation Gross Primary Production, Remote Sensing, 14, 6062, https://doi.org/10.3390/rs14236062, 2022.

Hurtt, G. C., Chini, L., Sahajpal, R., Frolking, S., Bodirsky, B. L., Calvin, K., Doelman, J. C., Fisk, J., Fujimori, S., Klein Goldewijk, K., Hasegawa, T., Havlik, P., Heinimann, A., Humpenöder, F., Jungclaus, J., Kaplan, J. O., Kennedy, J., Krisztin, T., Lawrence, D., Lawrence, P., Ma, L., Mertz, O., Pongratz, J., Popp, A., Poulter, B., Riahi, K., Shevliakova, E., Stehfest, E., Thornton, P., Tubiello, F. N., Van Vuuren, D. P., and Zhang, X.: Harmonization of global land use change and management for the period 850–2100 (LUH2) for CMIP6, Geosci. Model Dev., 13, 5425–5464, https://doi.org/10.5194/gmd-13-5425-2020, 2020.

Ibrom, A., Pilegaard, K., ICOS Ecosystem Thematic Centre, and Trotta, C.: Warm winter 2020 ecosystem eddy covariance flux product from Soroe (1.0), https://doi.org/10.18160/X4DF-R4S2, 2022.

https://doi.org/10.5194/essd-2026-796
Preprint. Discussion started: 13 November 2026
© Author(s) 2026. CC BY 4.0 License.



839 Iglewicz, B. and Hoaglin, D. C.: How to detect and handle outliers, ASQC Quality Press, Milwaukee, Wis, 87 pp.,
840 ISBN 978-0-87389-247-6, 1993.

841 Janssens, I., De Meulder, T., Roland, M., Segers, J., ICOS Ecosystem Thematic Centre, and Trotta, C.: Warm
842 winter 2020 ecosystem eddy covariance flux product from Brasschaat (1.0), https://doi.org/10.18160/YVBQ-
843 K6WF, 2022.

844 Keenan, T. F.: The FLUXNET Data Explorer (v1.0.0), https://doi.org/10.5281/ZENODO.20331228, 2026.

845 Kljun, N., Calanca, P., Rotach, M. W., and Schmid, H. P.: A simple two-dimensional parameterisation for Flux
846 Footprint Prediction (FFP), Geosci. Model Dev., 8, 3695–3713, https://doi.org/10.5194/gmd-8-3695-2015, 2015.

847 Knohl, A., Siebicke, L., Tiedemann, F., Kolle, O., ICOS Ecosystem Thematic Centre, and Trotta, C.: Warm winter
848 2020 ecosystem eddy covariance flux product from Hainich (1.0), https://doi.org/10.18160/CR66-PJ24, 2022.

849 Kobayashi, H. and Suzuki, R.: FLUXNET2015 US-Prr Poker Flat Research Range Black Spruce Forest,
850 https://doi.org/10.18140/FLX/1440113, 2016.

851 Kolari, P., Sahoo, G., Peltola, O., Keronen, P., ICOS Ecosystem Thematic Centre, and Trotta, C.: Warm winter
852 2020 ecosystem eddy covariance flux product from Varrio (1.0), https://doi.org/10.18160/0WR7-EQDP, 2022.

853 Kotani, A.: FLUXNET2015 JP-MBF Moshiri Birch Forest Site, https://doi.org/10.18140/FLX/1440238, 2016a.

854 Kotani, A.: FLUXNET2015 JP-SMF Seto Mixed Forest Site, https://doi.org/10.18140/FLX/1440239, 2016b.

855 Kowalska, N., Havrankova, K., Czerný, R., ICOS Ecosystem Thematic Centre, and Trotta, C.: Warm winter 2020
856 ecosystem eddy covariance flux product from Lanzhot (1.0), https://doi.org/10.18160/4HZC-4JSG, 2022.

857 Krinner, G., Viovy, N., De Noblet-Ducoudré, N., Ogée, J., Polcher, J., Friedlingstein, P., Ciais, P., Sitch, S., and
858 Prentice, I. C.: A dynamic global vegetation model for studies of the coupled atmosphere-biosphere system,
859 Global Biogeochemical Cycles, 19, 2003GB002199, https://doi.org/10.1029/2003GB002199, 2005.

860 Kuppel, S., Peylin, P., Maignan, F., Chevallier, F., Kiely, G., Montagnani, L., and Cescatti, A.: Model–data fusion
861 across ecosystems: from multisite optimizations to global simulations, Geosci. Model Dev., 7, 2581–2597,
862 https://doi.org/10.5194/gmd-7-2581-2014, 2014.

https://doi.org/10.5194/essd-2026-796
Preprint. Discussion started: 13 November 2026
© Author(s) 2026. CC BY 4.0 License.

Kutsch, W. L., Merbold, L., and Kolle, O.: FLUXNET2015 ZM-Mon Mongu, https://doi.org/10.18140/FLX/1440189, 2016.

Lardy, R., Bellocchi, G., and Soussana, J.-F.: A new method to determine soil organic carbon equilibrium, Environmental Modelling & Software, S1364815211001459, https://doi.org/10.1016/j.envsoft.2011.05.016, 2011.

Law, B.: FLUXNET2015 US-Me2 Metolius mature ponderosa pine, https://doi.org/10.18140/FLX/1440079, 2016a.

Law, B.: FLUXNET2015 US-Me6 Metolius Young Pine Burn, https://doi.org/10.18140/FLX/1440099, 2016b.

Liddell, M. J.: FLUXNET2015 AU-Rob Robson Creek, Queensland, Australia, https://doi.org/10.18140/FLX/1440203, 2016.

Lindauer, M., Steinbrecher, R., Wolpert, B., Mauder, M., and Schmid, H. P.: FLUXNET2015 DE-Lkb Lackenberg, https://doi.org/10.18140/FLX/1440214, 2016.

Lohila, A., Aurela, M., Tuovinen, J.-P., Hatakka, J., and Laurila, T.: FLUXNET2015 FI-Jok Jokioinen, https://doi.org/10.18140/FLX/1440159, 2016.

Loubet, B., Buysse, P., ICOS Ecosystem Thematic Centre, and Trotta, C.: Warm winter 2020 ecosystem eddy covariance flux product from Grignon (1.0), https://doi.org/10.18160/8XJC-HT7V, 2022.

Loustau, D., Chipeaux, C., ICOS Ecosystem Thematic Centre, and Trotta, C.: Warm winter 2020 ecosystem eddy covariance flux product from Bilos (1.0), https://doi.org/10.18160/MSRT-T1YA, 2022.

MacBean, N., Bacour, C., Raoult, N., Bastrikov, V., Koffi, E. N., Kuppel, S., Maignan, F., Ottlé, C., Peaucelle, M., Santaren, D., and Peylin, P.: Quantifying and Reducing Uncertainty in Global Carbon Cycle Predictions: Lessons and Perspectives From 15 Years of Data Assimilation Studies With the ORCHIDEE Terrestrial Biosphere Model, Global Biogeochemical Cycles, 36, e2021GB007177, https://doi.org/10.1029/2021GB007177, 2022.

Macfarlane, C., Lambert, P., Byrne, J., Johnstone, C., and Smart, N.: FLUXNET2015 AU-Gin Gingin, https://doi.org/10.18140/FLX/1440199, 2016a.

https://doi.org/10.5194/essd-2026-796
Preprint. Discussion started: 13 November 2026
© Author(s) 2026. CC BY 4.0 License.

Macfarlane, C., Prober, S., and Wiehl, G.: FLUXNET2015 AU-GWW Great Western Woodlands, Western Australia, Australia, https://doi.org/10.18140/FLX/1440200, 2016b.

Mammarella, I., Vesala, T., Kolari, P., ICOS Ecosystem Thematic Centre, and Trotta, C.: Warm winter 2020 ecosystem eddy covariance flux product from Hyytiälä (1.0), https://doi.org/10.18160/XTBV-XCJV, 2022.

Manca, G. and Goded, I.: FLUXNET2015 IT-PT1 Parco Ticino forest, https://doi.org/10.18140/FLX/1440172, 2016.

Margolis, H. A.: FLUXNET2015 CA-Qfo Quebec - Eastern Boreal, Mature Black Spruce, https://doi.org/10.18140/FLX/1440045, 2016.

Marie, G., Luyssaert, B. S., Dardel, C., Le Toan, T., Bouvet, A., Mermoz, S., Villard, L., Bastrikov, V., and Peylin, P.: Constraining a land cover map with satellite-based aboveground biomass estimates over Africa, Geosci. Model Dev., 15, 2599–2617, https://doi.org/10.5194/gmd-15-2599-2022, 2022.

Massman, B.: FLUXNET2015 US-GLE GLEES, https://doi.org/10.18140/FLX/1440069, 2016.

Matteucci, G.: FLUXNET2015 IT-Col Collelongo, https://doi.org/10.18140/FLX/1440167, 2016.

Meyer, W., Cale, P., Koerber, G., Ewenz, C., and Sun, Q.: FLUXNET2015 AU-Cpr Calperum, https://doi.org/10.18140/FLX/1440195, 2016.

Meyers, T.: AmeriFlux US-WBW Walker Branch Watershed, https://doi.org/10.17190/AMF/1246109, 2016.

Migliavacca, M., El-Madany, T. S., Carrara, A., Reichstein, M., ICOS Ecosystem Thematic Centre, and Trotta, C.: Warm winter 2020 ecosystem eddy covariance flux product from Majadas del Tietar North (1.0), https://doi.org/10.18160/J5YA-QZR1, 2022.

Moffat, A. M., Papale, D., Reichstein, M., Hollinger, D. Y., Richardson, A. D., Barr, A. G., Beckstein, C., Braswell, B. H., Churkina, G., Desai, A. R., Falge, E., Gove, J. H., Heimann, M., Hui, D., Jarvis, A. J., Kattge, J., Noormets, A., and Stauch, V. J.: Comprehensive comparison of gap-filling techniques for eddy covariance net carbon fluxes, Agricultural and Forest Meteorology, 147, 209–232, https://doi.org/10.1016/j.agrformet.2007.08.011, 2007.

https://doi.org/10.5194/essd-2026-796
Preprint. Discussion started: 13 November 2026
© Author(s) 2026. CC BY 4.0 License.

Mölder, M., Lankreijer, H., Lagergren, F., Holst, J., ICOS Ecosystem Thematic Centre, and Trotta, C.: Warm winter 2020 ecosystem eddy covariance flux product from Norunda (1.0), https://doi.org/10.18160/87R1-0HRM, 2022.

Montagnani, L., Stecher, M., ICOS Ecosystem Thematic Centre, and Trotta, C.: Warm winter 2020 ecosystem eddy covariance flux product from Renon (1.0), https://doi.org/10.18160/WMCA-8P4P, 2022.

Moors, E. and Elbers, J.: FLUXNET2015 NL-Loo Loobos, https://doi.org/10.18140/FLX/1440178, 2016.

Munger, J. W.: FLUXNET2015 US-Ha1 Harvard Forest EMS Tower (HFR1), https://doi.org/10.18140/FLX/1440071, 2016.

NEON (National Ecological Observatory Network): AmeriFlux FLUXNET-1F US-xBN NEON Caribou Creek - Poker Flats Watershed (BONA), https://doi.org/10.17190/AMF/2229406, 2023a.

NEON (National Ecological Observatory Network): AmeriFlux FLUXNET-1F US-xDJ NEON Delta Junction (DEJU), https://doi.org/10.17190/AMF/2229407, 2023b.

NEON (National Ecological Observatory Network): AmeriFlux FLUXNET-1F US-xRM NEON Rocky Mountain National Park, CASTNET (RMNP), https://doi.org/10.17190/AMF/1985450, 2023c.

NEON (National Ecological Observatory Network): AmeriFlux FLUXNET-1F US-xYE NEON Yellowstone Northern Range (Frog Rock) (YELL), https://doi.org/10.17190/AMF/1985459, 2023d.

Novick, K. and Phillips, R.: FLUXNET2015 US-MMS Morgan Monroe State Forest, https://doi.org/10.18140/FLX/1440083, 2016.

Olesen, J.: FLUXNET2015 DK-Fou Foulum, https://doi.org/10.18140/FLX/1440154, 2016.

Olivera-Guerra, L.-E., Ottlé, C., Raoult, N., and Peylin, P.: Assimilating ESA CCI land surface temperature into the ORCHIDEE land surface model: insights from a multi-site study across Europe, Hydrol. Earth Syst. Sci., 29, 261–290, https://doi.org/10.5194/hess-29-261-2025, 2025.

Ourcival, J.-M.: FLUXNET2015 FR-Pue Puechabon, https://doi.org/10.18140/FLX/1440164, 2016.

https://doi.org/10.5194/essd-2026-796
Preprint. Discussion started: 13 November 2026
© Author(s) 2026. CC BY 4.0 License.



Papale, D., Tirone, G., Valentini, R., Arriga, N., Belelli, L., Consalvo, C., Dore, S., Manca, G., Mazzenga, F., Sabbatini, S., and Stefani, P.: FLUXNET2015 IT-Ro2 Roccarespampani 2, https://doi.org/10.18140/FLX/1440175, 2016.

Pastorello, G., Trotta, C., Canfora, E., Chu, H., Christianson, D., Cheah, Y.-W., Poindexter, C., Chen, J., Elbashandy, A., Humphrey, M., Isaac, P., Polidori, D., Reichstein, M., Ribeca, A., Van Ingen, C., Vuichard, N., Zhang, L., Amiro, B., Ammann, C., Arain, M. A., Ardö, J., Arkebauer, T., Arndt, S. K., Arriga, N., Aubinet, M., Aurela, M., Baldocchi, D., Barr, A., Beamesderfer, E., Marchesini, L. B., Bergeron, O., Beringer, J., Bernhofer, C., Berveiller, D., Billesbach, D., Black, T. A., Blanken, P. D., Bohrer, G., Boike, J., Bolstad, P. V., Bonal, D., Bonnefond, J.-M., Bowling, D. R., Bracho, R., Brodeur, J., Brümmer, C., Buchmann, N., Burban, B., Burns, S. P., Buysse, P., Cale, P., Cavagna, M., Cellier, P., Chen, S., Chini, I., Christensen, T. R., Cleverly, J., Collalti, A., Consalvo, C., Cook, B. D., Cook, D., Coursolle, C., Cremonese, E., Curtis, P. S., D'Andrea, E., Da Rocha, H., Dai, X., Davis, K. J., Cinti, B. D., Grandcourt, A. D., Ligne, A. D., De Oliveira, R. C., Delpierre, N., Desai, A. R., Di Bella, C. M., Tommasi, P. D., Dolman, H., Domingo, F., Dong, G., Dore, S., Duce, P., Dufrêne, E., Dunn, A., Dušek, J., Eamus, D., Eichelmann, U., ElKhidir, H. A. M., Eugster, W., Ewenz, C. M., Ewers, B., Famulari, D., Fares, S., Feigenwinter, I., Feitz, A., Fensholt, R., Filippa, G., Fischer, M., Frank, J., Galvagno, M., Gharun, M., Gianelle, D., Gielen, B., Gioli, B., Gitelson, A., Goded, I., Goeckede, M., Goldstein, A. H., Gough, C. M., Goulden, M. L., Graf, A., Griebel, A., Gruening, C., Grünwald, T., Hammerle, A., Han, S., Han, X., Hansen, B. U., Hanson, C., Hatakka, J., He, Y., Hehn, M., Heinesch, B., Hinko-Najera, N., Hörtnagl, L., Hutley, L., Ibrom, A., Ikawa, H., Jackowicz-Korczynski, M., Janouš, D., Jans, W., Jassal, R., Jiang, S., Kato, T., Khomik, M., Klatt, J., Knohl, A., Knox, S., Kobayashi, H., Koerber, G., Kolle, O., Kosugi, Y., Kotani, A., Kowalski, A., Kruijt, B., Kurbatova, J., Kutsch, W. L., Kwon, H., Launiainen, S., Laurila, T., Law, B., Leuning, R., Li, Y., Liddell, M., Limousin, J.-M., Lion, M., Liska, A. J., Lohila, A., López-Ballesteros, A., López-Blanco, E., Loubet, B., Loustau, D., Lucas-Moffat, A., Lüers, J., Ma, S., Macfarlane, C., Magliulo, V., Maier, R., Mammarella, I., Manca, G., Marcolla, B., Margolis, H. A., Marras, S., Massman, W., Mastepanov, M., Matamala, R., Matthes, J. H., Mazzenga, F., McCaughey, H., McHugh, I., McMillan, A. M. S., Merbold, L., Meyer, W., Meyers, T., Miller, S. D., Minerbi, S., Moderow, U., Monson, R. K., Montagnani, L., Moore, C. E., Moors, E., Moreaux, V., Moureaux, C., Munger, J. W., Nakai, T., Neirynck, J., Nesic, Z., Nicolini, G., Noormets, A., Northwood, M., Nosetto, M., Nouvellon, Y., Novick, K., Oechel, W., Olesen, J. E., Ourcival, J.-M., Papuga, S. A., Parmentier, F.-J., Paul-Limoges, E., Pavelka, M., Peichl, M., Pendall, E., Phillips, R. P., Pilegaard, K., Pirk, N., Posse, G., Powell, T., Prasse, H., Prober, S. M., Rambal, S., Rannik, Ü., Raz-Yaseef, N., Rebmann, C., Reed, D., Dios, V. R. D., Restrepo-Coupe, N., Reverter, B. R., Roland, M., Sabbatini, S., Sachs, T., Saleska, S. R., Sánchez-Cañete, E. P., Sanchez-Mejia, Z. M., Schmid, H. P., Schmidt, M., Schneider, K., Schrader,

F., Schroder, I., Scott, R. L., Sedlák, P., Serrano-Ortíz, P., Shao, C., Shi, P., Shironya, I., Siebicke, L., Šigut, L., Silberstein, R., Sirca, C., Spano, D., Steinbrecher, R., Stevens, R. M., Sturtevant, C., Suyker, A., Tagesson, T., Takanashi, S., Tang, Y., Tapper, N., Thom, J., Tomassucci, M., Tuovinen, J.-P., Urbanski, S., Valentini, R., Van Der Molen, M., Van Gorsel, E., Van Huissteden, K., Varlagin, A., Verfaillie, J., Vesala, T., Vincke, C., Vitale, D., Vygodskaya, N., Walker, J. P., Walter-Shea, E., Wang, H., Weber, R., Westermann, S., Wille, C., Wofsy, S., Wohlfahrt, G., Wolf, S., Woodgate, W., Li, Y., Zampedri, R., Zhang, J., Zhou, G., Zona, D., Agarwal, D., Biraud, S., Torn, M., and Papale, D.: The FLUXNET2015 dataset and the ONEFlux processing pipeline for eddy covariance data, Sci Data, 7, 225, https://doi.org/10.1038/s41597-020-0534-3, 2020.

Peaucelle, M., Bacour, C., Ciais, P., Vuichard, N., Kuppel, S., Peñuelas, J., Belelli Marchesini, L., Blanken, P. D., Buchmann, N., Chen, J., Delpierre, N., Desai, A. R., Dufrene, E., Gianelle, D., Gimeno-Colera, C., Gruening, C., Helfter, C., Hörtnagl, L., Ibrom, A., Joffre, R., Kato, T., Kolb, T. E., Law, B., Lindroth, A., Mammarella, I., Merbold, L., Minerbi, S., Montagnani, L., Šigut, L., Sutton, M., Varlagin, A., Vesala, T., Wohlfahrt, G., Wolf, S., Yakir, D., and Viovy, N.: Covariations between plant functional traits emerge from constraining parameterization of a terrestrial biosphere model, Global Ecol Biogeogr, 28, 1351–1365, https://doi.org/10.1111/geb.12937, 2019.

Peichl, M., Nilsson, M. B., Pilegaard, K., de Simon, G., ICOS Ecosystem Thematic Centre, and Trotta, C.: Warm winter 2020 ecosystem eddy covariance flux product from Rosinedal-3 (1.0), https://doi.org/10.18160/RJ1S-CC2Z, 2022a.

Peichl, M., Ottosson Lofvenius, M., Nilsson, M. B., Marklund, P., ICOS Ecosystem Thematic Centre, and Trotta, C.: Warm winter 2020 ecosystem eddy covariance flux product from Svartberget (1.0), https://doi.org/10.18160/XWNX-9FWC, 2022b.

Pendall, E. and Griebel, A.: FLUXNET2015 AU-Cum Cumberland Plains, https://doi.org/10.18140/FLX/1440196, 2016.

Peylin, P., Bacour, C., MacBean, N., Leonard, S., Rayner, P., Kuppel, S., Koffi, E., Kane, A., Maignan, F., Chevallier, F., Ciais, P., and Prunet, P.: A new stepwise carbon cycle data assimilation system using multiple data streams to constrain the simulated land surface carbon cycle, Geosci. Model Dev., 9, 3321–3346, https://doi.org/10.5194/gmd-9-3321-2016, 2016.

Posse, G., Lewczuk, N., Richter, K., and Cristiano, P.: FLUXNET2015 AR-Vir Virasoro, https://doi.org/10.18140/FLX/1440192, 2016.

© Author(s) 2026. CC BY 4.0 License.


993 Post, H., Vrugt, J. A., Fox, A., Vereecken, H., and Hendricks Franssen, H.: Estimation of Community Land Model
994 parameters for an improved assessment of net carbon fluxes at European sites, JGR Biogeosciences, 122,
995 661–689, https://doi.org/10.1002/2015JG003297, 2017.

996 Poulter, B., MacBean, N., Hartley, A., Khlystova, I., Arino, O., Betts, R., Bontemps, S., Boettcher, M., Brockmann,
997 C., Defourny, P., Hagemann, S., Herold, M., Kirches, G., Lamarche, C., Lederer, D., Ottlé, C., Peters, M., and
998 Peylin, P.: Plant functional type classification for earth system models: results from the European Space
999 Agency's Land Cover Climate Change Initiative, Geosci. Model Dev., 8, 2315–2328,
1000 https://doi.org/10.5194/gmd-8-2315-2015, 2015.

1001 Poveda, F. D., Perez-Priego, O., Sanchez-Canete, E. P., Lopez Ballesteros, A., ICOS Ecosystem Thematic Centre,
1002 and Trotta, C.: Warm winter 2020 ecosystem eddy covariance flux product from Aguamarga (1.0),
1003 https://doi.org/10.18160/3V53-5P08, 2022.

1004 Prentice, I. C., Cramer, W., Harrison, S. P., Leemans, R., Monserud, R. A., and Solomon, A. M.: Special Paper: A
1005 Global Biome Model Based on Plant Physiology and Dominance, Soil Properties and Climate, Journal of
1006 Biogeography, 19, 117, https://doi.org/10.2307/2845499, 1992.

1007 Raoult, N., Douglas, N., MacBean, N., Kolassa, J., Quaife, T., Roberts, A. G., Fisher, R., Fer, I., Bacour, C., Dagon,
1008 K., Hawkins, L., Carvalhais, N., Cooper, E., Dietze, M. C., Gentine, P., Kaminski, T., Kennedy, D., Liddy, H. M.,
1009 Moore, D. J. P., Peylin, P., Pinnington, E., Sanderson, B., Scholze, M., Seiler, C., Smallman, T. L., Vergopolan, N.,
1010 Viskari, T., Williams, M., and Zobitz, J.: Parameter Estimation in Land Surface Models: Challenges and
1011 Opportunities With Data Assimilation and Machine Learning, J Adv Model Earth Syst, 17, e2024MS004733,
1012 https://doi.org/10.1029/2024MS004733, 2025.

1013 Raoult, N. M., Jupp, T. E., Cox, P. M., and Luke, C. M.: Land-surface parameter optimisation using data
1014 assimilation techniques: the adJULES system V1.0, Geosci. Model Dev., 9, 2833–2852,
1015 https://doi.org/10.5194/gmd-9-2833-2016, 2016.

1016 Rebmann, C., Dienstbach, L., Gimper, S., ICOS Ecosystem Thematic Centre, and Trotta, C.: Warm winter 2020
1017 ecosystem eddy covariance flux product from Hohes Holz (1.0), https://doi.org/10.18160/RRBD-7EME, 2022.

1018 Reichstein, M., Falge, E., Baldocchi, D., Papale, D., Aubinet, M., Berbigier, P., Bernhofer, C., Buchmann, N.,
1019 Gilmanov, T., Granier, A., Grünwald, T., Havránková, K., Ilvesniemi, H., Janous, D., Knohl, A., Laurila, T., Lohila,

© Author(s) 2026. CC BY 4.0 License.

A., Loustau, D., Matteucci, G., Meyers, T., Miglietta, F., Ourcival, J., Pumpanen, J., Rambal, S., Rotenberg, E., Sanz, M., Tenhunen, J., Seufert, G., Vaccari, F., Vesala, T., Yakir, D., and Valentini, R.: On the separation of net ecosystem exchange into assimilation and ecosystem respiration: review and improved algorithm, Global Change Biology, 11, 1424–1439, https://doi.org/10.1111/j.1365-2486.2005.001002.x, 2005.

Reick, C. H., Raddatz, T., Brovkin, V., and Gayler, V.: Representation of natural and anthropogenic land cover change in MPI-ESM, J Adv Model Earth Syst, 5, 459–482, https://doi.org/10.1002/jame.20022, 2013.

Reverter, B. R., Perez-Cañete, E. S., and Kowalski, A. S.: FLUXNET2015 ES-LgS Laguna Seca, https://doi.org/10.18140/FLX/1440225, 2016a.

Reverter, B. R., Perez-Cañete, E. S., and Kowalski, A. S.: FLUXNET2015 ES-Ln2 Lanjaron-Salvage logging, https://doi.org/10.18140/FLX/1440226, 2016b.

Reynolds, C. A., Jackson, T. J., and Rawls, W. J.: Estimating soil water-holding capacities by linking the Food and Agriculture Organization Soil map of the world with global pedon databases and continuous pedotransfer functions, Water Resources Research, 36, 3653–3662, https://doi.org/10.1029/2000WR900130, 2000.

Rubel, F., Brugger, K., Haslinger, K., and Auer, I.: The climate of the European Alps: Shift of very high resolution Köppen-Geiger climate zones 1800–2100, metz, 26, 115–125, https://doi.org/10.1127/metz/2016/0816, 2017.

Sabbatini, S., Arriga, N., Gioli, B., and Papale, D.: FLUXNET2015 IT-CA2 Castel d'Asso2, https://doi.org/10.18140/FLX/1440231, 2016.

Sanchez-Canete, E. P., Moya Jimenez, M. R., Czerný, R., Perez-Priego, O., ICOS Ecosystem Thematic Centre, and Trotta, C.: Warm winter 2020 ecosystem eddy covariance flux product from Llano de los Juanes (1.0), https://doi.org/10.18160/04BF-3AFE, 2022.

Santaren, D., Peylin, P., Viovy, N., and Ciais, P.: Optimizing a process-based ecosystem model with eddy-covariance flux measurements: A pine forest in southern France, Global Biogeochemical Cycles, 21, 2006GB002834, https://doi.org/10.1029/2006GB002834, 2007.

Schmid, H. P.: Footprint modeling for vegetation atmosphere exchange studies: a review and perspective, Agricultural and Forest Meteorology, 113, 159–183, https://doi.org/10.1016/S0168-1923(02)00107-7, 2002.

© Author(s) 2026. CC BY 4.0 License.

Schmidt, M., Graf, A., Dolfus, D., ICOS Ecosystem Thematic Centre, and Trotta, C.: Warm winter 2020 ecosystem eddy covariance flux product from Rollesbroich (1.0), https://doi.org/10.18160/Q02V-HAN4, 2022a.

Schmidt, M., Graf, A., Dolfus, D., ICOS Ecosystem Thematic Centre, and Trotta, C.: Warm winter 2020 ecosystem eddy covariance flux product from Selhausen Juelich (1.0), https://doi.org/10.18160/BS3C-CVQ0, 2022b.

Schmidt, M., Graf, A., Drüe, C., Dolfus, D., ICOS Ecosystem Thematic Centre, and Trotta, C.: Warm winter 2020 ecosystem eddy covariance flux product from Wustebach (1.0), https://doi.org/10.18160/JX9W-FBEJ, 2022c.

Schneider, K. and Schmidt, M.: FLUXNET2015 DE-Seh Selhausen, https://doi.org/10.18140/FLX/1440217, 2016.

Scholes, B.: FLUXNET2015 ZA-Kru Skukuza, https://doi.org/10.18140/FLX/1440188, 2016.

Schroder, I., Zegelin, S., Palu, T., and Feitz, A.: FLUXNET2015 AU-Emr Emerald, https://doi.org/10.18140/FLX/1440198, 2016.

Scott, R.: FLUXNET2015 US-SRG Santa Rita Grassland, https://doi.org/10.18140/FLX/1440114, 2016a.

Scott, R.: FLUXNET2015 US-SRM Santa Rita Mesquite, https://doi.org/10.18140/FLX/1440090, 2016b.

Scott, R.: FLUXNET2015 US-Whs Walnut Gulch Lucky Hills Shrub, https://doi.org/10.18140/FLX/1440097, 2016c.

Scott, R.: FLUXNET2015 US-Wkg Walnut Gulch Kendall Grasslands, https://doi.org/10.18140/FLX/1440096, 2016d.

Shi, J., Yuan, H., Lin, W., Dong, W., Liang, H., Liu, Z., Zeng, J., Zhang, H., Wei, N., Wei, Z., Zhang, S., Liu, S., Lu, X., and Dai, Y.: A flux tower site attribute dataset intended for land surface modeling, Earth Syst. Sci. Data, 17, 117–134, https://doi.org/10.5194/essd-17-117-2025, 2025.

Shi, P., Zhang, X., and He, Y.: FLUXNET2015 CN-Dan Dangxiong, https://doi.org/10.18140/FLX/1440138, 2016.

Sigut, L., Havrankova, K., Jocher, G., Pavelka, M., and Janouš, D.: FLUXNET2015 CZ-BK2 Bily Kriz grassland, https://doi.org/10.18140/FLX/1440144, 2016.

© Author(s) 2026. CC BY 4.0 License.



1069 Sigut, L., Foltýnová, L., Kowalska, N., Pavelka, M., ICOS Ecosystem Thematic Centre, and Trotta, C.: Warm
1070 winter 2020 ecosystem eddy covariance flux product from Bily Kriz forest (1.0),
1071 https://doi.org/10.18160/2X51-1SD0, 2022a.

1072 Sigut, L., Foltýnová, L., Czerný, R., Pavelka, M., ICOS Ecosystem Thematic Centre, and Trotta, C.: Warm winter
1073 2020 ecosystem eddy covariance flux product from Rajec (1.0), https://doi.org/10.18160/AAYD-C9FK, 2022b.

1074 Sigut, L., Foltýnová, L., Czerný, R., Pavelka, M., ICOS Ecosystem Thematic Centre, and Trotta, C.: Warm winter
1075 2020 ecosystem eddy covariance flux product from Stitna (1.0), https://doi.org/10.18160/0JY0-ZCD6, 2022c.

1076 Simioni, G., Marloie, O., Guibal, F., ICOS Ecosystem Thematic Centre, and Trotta, C.: Warm winter 2020
1077 ecosystem eddy covariance flux product from Font-Blanche (1.0), https://doi.org/10.18160/KGN6-K1CX, 2022.

1078 Spano, D., Duce, P., Marras, S., Sirca, C., Arca, A., Zara, P., and Ventura, A.: FLUXNET2015 IT-Noe Arca di Noe -
1079 Le Prigionette, https://doi.org/10.18140/FLX/1440171, 2016.

1080 Still, C. J., Berry, J. A., Collatz, G. J., Defries, R. S., Hall, F. G., Meeson, B. W., Los, S. O., Brown de Colstoun, E.,
1081 and Landis, D. R.: International Satellite Land Surface Climatology Project (ISLSCP II)ISLSCP II C4 Vegetation
1082 Percentage, https://doi.org/10.3334/ORNLDAAC/932, 1 January 2009., 2009.

1083 Stöckli, R., Lawrence, D. M., Niu, G. -Y., Oleson, K. W., Thornton, P. E., Yang, Z. -L., Bonan, G. B., Denning, A. S.,
1084 and Running, S. W.: Use of FLUXNET in the Community Land Model development, J. Geophys. Res., 113,
1085 2007JG000562, https://doi.org/10.1029/2007JG000562, 2008.

1086 Suyker, A.: FLUXNET2015 US-Ne1 Mead - irrigated continuous maize site,
1087 https://doi.org/10.18140/FLX/1440084, 2016.

1088 Szutu, D. and Baldocchi, D.: FLUXNET2015 US-Tw3 Twitchell Alfalfa, https://doi.org/10.18140/FLX/1440110,
1089 2016.

1090 Tang, Y., Kato, T., and Du, M.: FLUXNET2015 CN-HaM Haibei Alpine Tibet site,
1091 https://doi.org/10.18140/FLX/1440190, 2016.

© Author(s) 2026. CC BY 4.0 License.

Tartaglione, V., Cédric Bacour, and Fabienne Maignan: A database with refined plant functional type attribution at eddy covariance sites for enhanced land surface model simulations, https://doi.org/10.14768/6e99ff4b-3205-4038-8f9a-713e3e33753d, 2026.

Taylor, K. E.: Summarizing multiple aspects of model performance in a single diagram, J. Geophys. Res., 106, 7183–7192, https://doi.org/10.1029/2000JD900719, 2001.

Torn, M.: FLUXNET2015 US-ARb ARM Southern Great Plains burn site- Lamont, https://doi.org/10.18140/FLX/1440064, 2016a.

Torn, M.: FLUXNET2015 US-ARc ARM Southern Great Plains control site- Lamont, https://doi.org/10.18140/FLX/1440065, 2016b.

Ukkola, A. M., Abramowitz, G., and De Kauwe, M. G.: A flux tower dataset tailored for land model evaluation, Earth Syst. Sci. Data, 14, 449–461, https://doi.org/10.5194/essd-14-449-2022, 2022.

Valentini, R., Dore, S., Mazzenga, F., Sabbatini, S., Stefani, P., Tirone, G., and Papale, D.: FLUXNET2015 IT-Cpz Castelporziano, https://doi.org/10.18140/FLX/1440168, 2016a.

Valentini, R., Tirone, G., Vitale, D., Papale, D., Arriga, N., Belelli, L., Dore, S., Manca, G., Mazzenga, F., Pegoraro, E., Sabbatini, S., and Stefani, P.: FLUXNET2015 IT-Ro1 Roccarespampani 1, https://doi.org/10.18140/FLX/1440174, 2016b.

Varlagin, A., Kurbatova, J., Vygodskaya, N., ICOS Ecosystem Thematic Centre, and Trotta, C.: Warm winter 2020 ecosystem eddy covariance flux product from Fyodorovskoye (1.0), https://doi.org/10.18160/XMER-D4NR, 2022a.

Varlagin, A., Kurbatova, J., Vygodskaya, N., ICOS Ecosystem Thematic Centre, and Trotta, C.: Warm winter 2020 ecosystem eddy covariance flux product from Fyodorovskoye dry spruce stand (1.0), https://doi.org/10.18160/WK2C-VM7N, 2022b.

Vincke, C., Heinesch, B., Longdoz, B., ICOS Ecosystem Thematic Centre, and Trotta, C.: Warm winter 2020 ecosystem eddy covariance flux product from Vielsalm (1.0), https://doi.org/10.18160/DF9X-QMRK, 2022.

Wang, H. and Fu, X.: FLUXNET2015 CN-Qia Qianyanzhou, https://doi.org/10.18140/FLX/1440141, 2016.

https://doi.org/10.5194/essd-2026-796
Preprint. Discussion started: 13 November 2026
© Author(s) 2026. CC BY 4.0 License.

Wang, L., Arora, V. K., Bartlett, P., Chan, E., and Curasi, S. R.: Mapping of ESA's Climate Change Initiative land cover data to plant functional types for use in the CLASSIC land model, Biogeosciences, 20, 2265–2282, https://doi.org/10.5194/bg-20-2265-2023, 2023.

Warm Winter 2020 Team, ICOS Ecosystem Thematic Centre, ICOS Ecosystem Thematic Centre, and Trotta, C.: Warm Winter 2020 ecosystem eddy covariance flux product for 73 stations in FLUXNET-Archive format—release 2022-1, https://doi.org/10.18160/2G60-ZHAK, 1 February 2022., 2022.

Williams, M., Richardson, A. D., Reichstein, M., Stoy, P. C., Peylin, P., Verbeeck, H., Carvalhais, N., Jung, M., Hollinger, D. Y., Kattge, J., Leuning, R., Luo, Y., Tomelleri, E., Trudinger, C. M., and Wang, Y.-P.: Improving land surface models with FLUXNET data, Biogeosciences, 6, 1341–1359, https://doi.org/10.5194/bg-6-1341-2009, 2009.

Wohlfahrt, G., Hammerle, A., and Hörtnagl, L.: FLUXNET2015 AT-Neu Neustift, https://doi.org/10.18140/FLX/1440121, 2016.

Woodgate, W., Van Gorsel, E., and Leuning, R.: FLUXNET2015 AU-Tum Tumbarumba, https://doi.org/10.18140/FLX/1440126, 2016.

Yakir, D., Muller, J., Schwartz, E., Rotenberg, E., ICOS Ecosystem Thematic Centre, and Trotta, C.: Warm winter 2020 ecosystem eddy covariance flux product from Yatir (1.0), https://doi.org/10.18160/MAGT-CWRW, 2022.

Zhang, J. and Han, S.: FLUXNET2015 CN-Cha Changbaishan, https://doi.org/10.18140/FLX/1440137, 2016.

Zhou, G. and Yan, J.: FLUXNET2015 CN-Din Dinghushan, https://doi.org/10.18140/FLX/1440139, 2016.

Appendix A

Table A1: Sites citations.

Site ID	Citation
AR-SLu	Garcia et al., 2016
AR-Vir	Posse et al., 2016
AT-Neu	Wohlfahrt et al., 2016

https://doi.org/10.5194/essd-2026-796
Preprint. Discussion started: 13 November 2026
© Author(s) 2026. CC BY 4.0 License.


AU-Ade	Beringer and Hutley, 2016a
AU-ASM	Cleverly and Eamus, 2016a
AU-Cpr	Meyer et al., 2016
AU-Cum	Pendall and Griebel, 2016
AU-DaP	Beringer and Hutley, 2016b
AU-DaS	Beringer and Hutley, 2016g
AU-Dry	Beringer and Hutley, 2016c
AU-Emr	Schroder et al., 2016
AU-Gin	Macfarlane et al., 2016a
AU-GWW	Macfarlane et al., 2016b
AU-How	Beringer and Hutley, 2016d
AU-Lox	Ewenz et al., 2016
AU-RDF	Beringer and Hutley, 2016e
AU-Rig	Beringer et al., 2016a
AU-Rob	Liddell, 2016
AU-Stp	Beringer and Hutley, 2016f
AU-TTE	Cleverly and Eamus, 2016b
AU-Tum	Woodgate et al., 2016
AU-Wac	Beringer et al., 2016b
AU-Whr	Beringer et al., 2016c
AU-Wom	Arndt et al., 2016
AU-Ync	Beringer and Walker, 2016
BE-Bra	Janssens et al., 2022
BE-Dor	Heinesch et al., 2022a
BE-Jal	Baldocchi et al., 2001
BE-Lon	Heinesch et al., 2022b
BE-Vie	Vincke et al., 2022
BR-Sa3	Goulden, 2016a

https://doi.org/10.5194/essd-2026-796
Preprint. Discussion started: 13 November 2026
© Author(s) 2026. CC BY 4.0 License.



BW-Ma1	Baldocchi et al., 2001
CA-Man	Amiro, 2016a
CA-NS1	Goulden, 2016b
CA-NS2	Goulden, 2016c
CA-NS3	Goulden, 2016d
CA-NS4	Goulden, 2016e
CA-NS5	Goulden, 2016f
CA-NS6	Goulden, 2016g
CA-NS7	Goulden, 2016h
CA-Qfo	Margolis, 2016
CA-SF1	Amiro, 2016b
CA-SF2	Amiro, 2016c
CA-SF3	Amiro, 2016d
CH-Aws	Buchmann et al., 2022a
CH-Cha	Buchmann et al., 2022b
CH-Dav	Buchmann et al., 2022c
CH-Fru	Buchmann et al., 2022d
CH-Lae	Buchmann et al., 2022e
CH-Oe1	Ammann, 2016
CN-Cha	Zhang and Han, 2016
CN-Cng	Dong, 2016
CN-Dan	Shi et al., 2016
CN-Din	Zhou and Yan, 2016
CN-Du2	Chen, 2016f
CN-HaM	Tang et al., 2016
CN-Qia	Wang and Fu, 2016
CZ-BK1	Sigut et al., 2022a
CZ-BK2	Sigut et al., 2016

https://doi.org/10.5194/essd-2026-796
Preprint. Discussion started: 13 November 2026
© Author(s) 2026. CC BY 4.0 License.



CZ-KrP	Acosta et al., 2022
CZ-Lnz	Kowalska et al., 2022
CZ-RAJ	Sigut et al., 2022b
CZ-Stn	Sigut et al., 2022c
DE-Bay	Baldocchi et al., 2001
DE-Geb	Bruemmer et al., 2022
DE-Gri	Bernhofer et al., 2022a
DE-Hai	Knohl et al., 2022
DE-HoH	Rebmann et al., 2022
DE-Hzd	Bernhofer et al., 2022b
DE-Kli	Bernhofer et al., 2022c
DE-Lkb	Lindauer et al., 2016
DE-Meh	Baldocchi et al., 2001
DE-Obe	Bernhofer et al., 2022d
DE-RuR	Schmidt et al., 2022a
DE-RuS	Schmidt et al., 2022b
DE-RuW	Schmidt et al., 2022c
DE-Seh	Schneider and Schmidt, 2016
DE-Tha	Bernhofer et al., 2022e
DE-Wet	Baldocchi et al., 2001
DK-Fou	Olesen, 2016
DK-Lva	Baldocchi et al., 2001
DK-Ris	Baldocchi et al., 2001
DK-Sor	Ibrom et al., 2022
ES-Abr	El-Madany et al., 2022a
ES-Agu	Poveda et al., 2022
ES-ES1	Baldocchi et al., 2001
ES-ES2	Baldocchi et al., 2001

https://doi.org/10.5194/essd-2026-796
Preprint. Discussion started: 13 November 2026
© Author(s) 2026. CC BY 4.0 License.



ES-LgS	Reverter et al., 2016a
ES-LJu	Sanchez-Canete et al., 2022
ES-LM1	Migliavacca et al., 2022
ES-LM2	El-Madany et al., 2022b
ES-LMa	Baldocchi et al., 2001
ES-Ln2	Reverter et al., 2016b
ES-VDA	Baldocchi et al., 2001
FI-Hyy	Mammarella et al., 2022
FI-Jok	Lohila et al., 2016
FI-Ken	Aurela et al., 2022
FI-Qvd	Heimsch et al., 2022
FI-Sod	Aurela et al., 2016
FI-Var	Kolari et al., 2022
FR-Bil	Loustau et al., 2022
FR-FBn	Simioni et al., 2022
FR-Fon	Dufrêne et al., 2022
FR-Gri	Loubet et al., 2022
FR-Hes	Cuntz et al., 2022
FR-LBr	Berbigier and Loustau, 2016
FR-Lq1	Baldocchi et al., 2001
FR-Lq2	Baldocchi et al., 2001
FR-Pue	Ourcival, 2016
FR-Tou	Calvet et al., 2022
GF-Guy	Bonal and Burban, 2022
HU-Bug	Baldocchi et al., 2001
HU-Mat	Baldocchi et al., 2001
ID-Pag	Baldocchi et al., 2001
IE-Ca1	Baldocchi et al., 2001

https://doi.org/10.5194/essd-2026-796
Preprint. Discussion started: 13 November 2026
© Author(s) 2026. CC BY 4.0 License.



IE-Dri	Baldocchi et al., 2001
IL-Yat	Yakir et al., 2022
IT-BFt	Gerosa et al., 2022
IT-CA2	Sabbatini et al., 2016
IT-Col	Matteucci, 2016
IT-Cp2	Fares et al., 2022
IT-Cpz	Valentini et al., 2016a
IT-Isp	Gruening et al., 2016a
IT-La2	Cescatti et al., 2016
IT-Lav	Gianelle et al., 2022a
IT-Lec	Baldocchi et al., 2001
IT-LMa	Baldocchi et al., 2001
IT-Mal	Baldocchi et al., 2001
IT-MBo	Gianelle et al., 2022b
IT-Noe	Spano et al., 2016
IT-Non	Baldocchi et al., 2001
IT-Pia	Baldocchi et al., 2001
IT-PT1	Manca and Goded, 2016
IT-Ren	Montagnani et al., 2022
IT-Ro1	Valentini et al., 2016b
IT-Ro2	Papale et al., 2016
IT-SR2	Arriga et al., 2022
IT-SRo	Gruening et al., 2016b
IT-Tor	Cremonese et al., 2022
JP-MBF	Kotani, 2016a
JP-SMF	Kotani, 2016b
NL-Ca1	Baldocchi et al., 2001
NL-Lan	Baldocchi et al., 2001

https://doi.org/10.5194/essd-2026-796
Preprint. Discussion started: 13 November 2026
© Author(s) 2026. CC BY 4.0 License.



NL-Loo	Moors and Elbers, 2016
NL-Lut	Baldocchi et al., 2001
NL-Mol	Baldocchi et al., 2001
PT-Esp	Baldocchi et al., 2001
PT-Mi1	Baldocchi et al., 2001
PT-Mi2	Baldocchi et al., 2001
RU-Cok	Dolman et al., 2016
RU-Fy2	Varlagin et al., 2022b
RU-Fyo	Varlagin et al., 2022a
RU-Ha1	Belelli et al., 2016
RU-Ha2	Baldocchi et al., 2001
RU-Ha3	Baldocchi et al., 2001
RU-Zot	Baldocchi et al., 2001
SD-Dem	Ardö et al., 2016
SE-Fla	Baldocchi et al., 2001
SE-Htm	Heliasz et al., 2022
SE-Nor	Mölder et al., 2022
SE-Ros	Peichl et al., 2022a
SE-Sk1	Baldocchi et al., 2001
SE-Sk2	Baldocchi et al., 2001
SE-Svb	Peichl et al., 2022b
UK-EBu	Baldocchi et al., 2001
UK-ESa	Baldocchi et al., 2001
UK-Gri	Baldocchi et al., 2001
UK-Ham	Baldocchi et al., 2001
UK-Her	Baldocchi et al., 2001
UK-PL3	Baldocchi et al., 2001
UK-Tad	Baldocchi et al., 2001

https://doi.org/10.5194/essd-2026-796
Preprint. Discussion started: 13 November 2026
© Author(s) 2026. CC BY 4.0 License.



US-AR1	Billesbach et al., 2016a
US-AR2	Billesbach et al., 2016b
US-ARb	Torn, 2016a
US-ARc	Torn, 2016b
US-ARM	Biraud et al., 2016
US-Aud	Baldocchi et al., 2001
US-Bar	Baldocchi et al., 2001
US-Bkg	Baldocchi et al., 2001
US-Blo	Goldstein, 2016
US-BZS	Euskirchen, 2022
US-Cop	Bowling, 2016
US-FPe	Baldocchi et al., 2001
US-GLE	Massman, 2016
US-Goo	Baldocchi et al., 2001
US-Ha1	Munger, 2016
US-Ho1	Baldocchi et al., 2001
US-Ho2	Baldocchi et al., 2001
US-KS2	Drake and Hinkle, 2016
US-Me2	Law, 2016a
US-Me4	Baldocchi et al., 2001
US-Me6	Law, 2016b
US-MMS	Novick and Phillips, 2016
US-MOz	Baldocchi et al., 2001
US-Ne1	Suyker, 2016
US-NR1	Blanken et al., 2016
US-Oho	Baldocchi et al., 2001
US-PFa	Desai, 2016a
US-Prr	Kobayashi and Suzuki, 2016

https://doi.org/10.5194/essd-2026-796
Preprint. Discussion started: 13 November 2026
© Author(s) 2026. CC BY 4.0 License.



US-SP1	Baldocchi et al., 2001
US-SP2	Baldocchi et al., 2001
US-SRG	Scott, 2016a
US-SRM	Scott, 2016b
US-Syv	Desai, 2016b
US-Ton	Baldocchi and Ma, 2016
US-Tw3	Szutu and Baldocchi, 2016
US-UMB	Gough et al., 2016a
US-UMd	Gough et al., 2016b
US-Var	Baldocchi et al., 2016
US-WBW	Meyers, 2016
US-WCr	Desai, 2016c
US-Whs	Scott, 2016c
US-Wi0	Chen, 2016a
US-Wi1	Baldocchi et al., 2001
US-Wi2	Baldocchi et al., 2001
US-Wi3	Chen, 2016b
US-Wi4	Chen, 2016c
US-Wi5	Baldocchi et al., 2001
US-Wi6	Chen, 2016d
US-Wi7	Baldocchi et al., 2001
US-Wi8	Baldocchi et al., 2001
US-Wi9	Chen, 2016e
US-Wkg	Scott, 2016d
US-xBN	NEON (National Ecological Observatory Network), 2023a
US-xDJ	NEON (National Ecological Observatory Network), 2023b
US-xRM	NEON (National Ecological Observatory Network), 2023c
US-xYE	NEON (National Ecological Observatory Network), 2023d

https://doi.org/10.5194/essd-2026-796
Preprint. Discussion started: 13 November 2026
© Author(s) 2026. CC BY 4.0 License.



Open Access Earth System Science Data Discussions

ZA-Kru	Scholes, 2016
ZM-Mon	Kutsch et al., 2016

1137